Cellular/Molecular

p140Cap Regulates the Composition and Localization of the NMDAR Complex in Synaptic Lipid Rafts

Costanza Angelini,[1*] Alessandro Morellato,[1*] Annalisa Alfieri,[1] Lisa Pavinato,[2] Tiziana Cravero,[1] Olga Teresa Bianciotto,[1] Vincenzo Salemme,[1] Dora Natalini,[1] Giorgia Centonze,[1] Alessandra Raspanti,[3] Tina Garofalo,[4] Donatella Valdembri,[5,6] Guido Serini,[5,6] Andrea Marcantoni,[7,8] Andrea Becchetti,[8] Maurizio Giustetto,[3] Emilia Turco,[1] and Paola Defilippi[1]

[1]Department of Molecular Biotechnology and Health Sciences, University of Torino, Torino, 10126, Italy, [2]Department of Medical Sciences, Medical Genetics Unit, University of Torino, Torino, 10126, Italy, [3]Neuroscience Department "Rita Levi Montalcini," University of Torino, Torino, 10125, Italy, [4]Department of Experimental Medicine, Sapienza University, Roma, 00161, Italy, [5]Department of Oncology, University of Torino School of Medicine, Regione Gonzole, 10, 10043, Orbassano, TO, Italy, [6]Candiolo Cancer Institute, FPO-IRCCS, Candiolo, Torino, 10060, Italy, [7]Department of Drug Science, Laboratory of Cellular and Molecular Neuroscience, University of Torino, Torino, 10126, Italy, and [8]Department of Biotechnology and Biosciences and NeuroMI, University of Milano-Bicocca, Milano, 20126, Italy

The NMDARs are key players in both physiological and pathologic synaptic plasticity because of their involvement in many aspects of neuronal transmission as well as learning and memory. The contribution in these events of different types of GluN2A-interacting proteins is still unclear. The p140Cap scaffold protein acts as a hub for postsynaptic complexes relevant to psychiatric and neurologic disorders and regulates synaptic functions, such as the stabilization of mature dendritic spine, memory consolidation, LTP, and LTD. Here we demonstrate that p140Cap directly binds the GluN2A subunit of NMDAR and modulates GluN2A-associated molecular network. Indeed, in p140Cap KO male mice, GluN2A is less associated with PSD95 both in *ex vivo* synaptosomes and in cultured hippocampal neurons, and p140Cap expression in KO neurons can rescue GluN2A and PSD95 colocalization. p140Cap is crucial in the recruitment of GluN2A-containing NMDARs and, consequently, in regulating NMDARs' intrinsic properties. p140Cap is associated to synaptic lipid-raft (LR) and to soluble postsynaptic membranes, and GluN2A and PSD95 are less recruited into synaptic LR of p140Cap KO male mice. Gated-stimulated emission depletion microscopy on hippocampal neurons confirmed that p140Cap is required for embedding GluN2A clusters in LR in an activity-dependent fashion. In the synaptic compartment, p140Cap influences the association between GluN2A and PSD95 and modulates GluN2A enrichment into LR. Overall, such increase in these membrane domains rich in signaling molecules results in improved signal transduction efficiency.

Key words: GluN2A; lipid raft; NMDAR; p140Cap; synaptic plasticity

Significance Statement

Here we originally show that the adaptor protein p140Cap directly binds the GluN2A subunit of NMDAR and modulates the GluN2A-associated molecular network. Moreover, we show, for the first time, that p140Cap also associates to synaptic lipid rafts and controls the selective recruitment of GluN2A and PSD95 to this specific compartment. Finally, gated-stimulated emission depletion microscopy on hippocampal neurons confirmed that p140Cap is required for embedding GluN2A clusters in lipid rafts in an activity-dependent fashion. Overall, our findings provide the molecular and functional dissection of p140Cap as a new active member of a highly dynamic synaptic network involved in memory consolidation, LTP, and LTD, which are known to be altered in neurologic and psychiatric disorders.

Received Sep. 24, 2021; revised June 7, 2022; accepted June 12, 2022.

Author contributions: C.A., A. Morellato, A. Marcantoni, A.B., E.T., and P.D. designed research; C.A., A. Morellato, O.T.B., and A. Marcantoni performed research; C.A., A.A., L.P., T.C., V.S., D.N., G.C., A.R., T.G., D.V., G.S., and M.G. contributed unpublished reagents/analytic tools; C.A., A. Morellato, A. Marcantoni, and A.B. analyzed data; C.A. and A. Morellato wrote the first draft of the paper; C.A., A. Morellato, E.T., and P.D. edited the paper; C.A., A. Morellato, A. Marcantoni, A. Morellato, E.T., and P.D. wrote the paper.

This work was supported by Ministero Università Ricerca PRIN 2015 to P.D.; Associazione Italiana Ricerca Cancro IG-20107 to P.D.; Compagnia San Paolo, Torino, Progetto DEFLECT to P.D.; Fondazione CRT 2020.1798 to P.D.; and RILO University of Torino (ex 60%) to P.D. and E.T. The laboratory of M.G. was supported by Ministero Università Ricerca project Dipartimenti di Eccellenza 2018-2022, Fondazione Intesa Sanpaolo, Fondazione CRT, and Fondazione Telethon Onlus. A.B. was supported by University of Milano-Bicocca 2021-ATE-0042. We thank Professor Fabrizio Gardoni (University of Milan) for GST-GluN2A constructs and for advice on c-LTP protocol; and Dr. Marta Gai (Open Lab of Advanced Microscopy at the Molecular Biotechnology Center) for support.

*C.A. and A. Morellato contributed equally to this work.

The authors declare no competing financial interests.

Correspondence should be addressed to Paola Defilippi at paola.defilippi@unito.it.

https://doi.org/10.1523/JNEUROSCI.1775-21.2022

Introduction

The dendritic spines (DSs) are specialized structures representing the locus of neuroexcitatory transmission and plasticity (Sala and Segal, 2014). The postsynaptic density (PSD) is housed on the top of the DS and consists of a thick electron-dense membrane-associated protein complex specialized for postsynaptic signaling and remodeling (Dosemeci et al., 2016). p140Cap is a scaffold protein of the PSD involved in the regulation of actin dynamic in the DS (Jaworski et al., 2009; Hayashi et al., 2011). Indeed, acute p140Cap silencing *in vitro* impacts on DS morphology by increasing the number of filopodial immature DS (Tomasoni et al., 2013). Accordingly, hippocampal neurons derived from p140Cap KO mice show reduced number of mature DS and increased number of filopodial DS (Repetto et al., 2014). The alteration in the phenotype of the DS observed in p140Cap KO mice correlates in the electrophysiological analysis with defective synaptic plasticity processes, namely, the LTP and the LTD, and with impaired memory consolidation in novel object recognition test (Repetto et al., 2014). LTP and LTD are believed to play a major role in learning and memory formation (Caroni et al., 2012; Holtmaat and Caroni, 2016), and alterations in these processes could be the result of alterations in ionotropic glutamate receptor (iGluR) activity (Moretto et al., 2018). At the molecular level, LTP and LTD are mediated by the NMDARs, a heterotetrameric iGluR composed of two obligatory GluN1 subunits and two modulatory GluN2 (A-D) subunits (Cull-Candy et al., 2001; Paoletti et al., 2013). The cytoplasmic tails of NMDAR subunits impart considerable bulk to the PSD (Tomasetti et al., 2017). Indeed, a specific set of molecules bind to the C-terminal region of GluN2 subunit of NMDAR forming a large multiprotein complex (Husi et al., 2000; Fan et al., 2014), which includes scaffold molecules, as the MAGUK family protein PSD95 (Zhu et al., 2016), signaling proteins as well as molecules associated to the lipid raft (LR) domains of the plasma membrane, such as Flotillin-1 (Swanwick et al., 2009).

LRs are membrane microdomains enriched in cholesterol and sphingolipids, endowed with signaling molecules (Brown and London, 1998; Simons and Toomre, 2000; Ikonen, 2001). Recent studies describe that NMDARs trafficking to LR are dynamically enhanced during both synaptic plasticity process and memory formation (Delint-Ramirez et al., 2008, 2010)

p140Cap is an adaptor protein; therefore, its role in the PSD could be explained by its ability to interact with specific partners. To identify such putative partners, we recently generated a p140Cap interactome in synaptosomes, and we found that GluN2A and GluN2B subunits of the NMDAR were comprised among the high-fidelity binding partners, indicating a potential involvement of p140Cap in glutamatergic transmission (Alfieri et al., 2017). The association of p140Cap with the NMDAR could thus impact on both LTP and LTD as well as on learning and memory, providing a molecular framework for the cognitive defects observed in p140Cap KO mice.

Here we show that p140Cap is a novel direct binding partner of the GluN2A subunit and that their association impacts on the composition of the GluN2A-associated molecular complex in synaptosomes. Moreover, p140Cap can modulate GluN2A-containing receptor recruitment and clustering into synaptic LR in an activity-dependent fashion, suggesting the relevance of p140Cap as a new molecule able to influence the GluN2A-containing NMDAR localization and activity into LR.

Materials and Methods

Animals. Mixed 129 Sv × C57BL/6J p140Cap heterozygous mice were used for breeding and generation of WT and p140Cap KO littermates, as previously described by Repetto et al. (2014). All experiments were approved and performed in accordance with the current Italian law in relation to animal use and protection in scientific research. Male, 3- to 4-month-old WT and *p140Cap KO* littermates were used for synaptosomes preparations. WT animals from p0 to p60 were used to perform time course experiments on telencephalon extracts. Animals were killed by cervical dislocation.

Antibodies. For Western blot (WB) analysis, the following antibodies were used: mouse monoclonal antibody (mAb) α-p140Cap (1:1000, 0.5 μg/ml), α-GFP polyclonal antibody (1:1000 pAb), α-GST (1:1000 mAb), α-MBP (1:1000 mAb) are home made in our Dept Antibody facility. α-Camk2β rabbit pAb antibody (1:1000 Abcam ab34703), α-CDC42 rabbit pAb antibody (1:1000 Cell Signaling 2462), α-Flotillin-1 rabbit pAb antibody (1:1000 Santa Cruz Biotechnology H-104), α-GAPDH mAb (1:8000 Millipore MAB374), α-GluN1 rabbit pAb (1:700 Thermo Fisher Scientific PA3-102), α-GluN2A rabbit pAb (1:1000 Thermo Fisher Scientific PA5-35377), α-GluN2B mAb (1:1000 NeuroMab 75-097), α-phospho-Ser 845-GluR1 (1:1000 Abcam ab76321), α-GluR1 (1:1000 Thermo Fisher Scientific), α-Gria2 rabbit pAb antibody (1:1000 Abcam ab20673), α-PSD95 mAb (1:1000 Abcam 2723), α-Rac1 mAb (1:2000 clone 23A8 Millipore), α-Src mAb (1:1000 Santa Cruz Biotechnology B_{12}), α-Tiam1 rabbit pAb (1:1000 Santa Cruz Biotechnology C-16), α-transferrin receptor-1 CD71 mAb (1:1000 Thermo Fisher Scientific H68.4), and α-Tubulin mAb (1:8000 Sigma-Aldrich T5168). Secondary antibodies conjugated with peroxidase were purchased from GE Healthcare. For immunofluorescence, slides were stained with α-p140Cap and α-p140Cap-647-conjugated mAb (1:500, see above), α GFP mAb (1:1000 Abcam), α-GluN2A rabbit pAb (1:300 Thermo Fisher Scientific PA5-35377), α-Bassoon (1:500 SynapticSystem 141003), α-PSD95 mAb (1:500 Abcam 2723), and α-Map2 chicken (1:1000 Abcam ab5392). Phalloidin-FITC or -647 was purchased from Sigma. Secondary antibodies conjugated with AlexaFluor-488, -568, or -647 (1:1000) were purchased from Invitrogen, Thermo Fisher Scientific.

DNA constructs. For expression in mammalian cells, full-length mouse p140Cap cDNA was cloned into the BamHI site of pCDNA3.1/Myc-Hys expression vector (Thermo Fisher Scientific) and sequenced. Full-length mouse p140Cap cDNA was cloned into the EcoRI-KpnI sites of pEGFP-N2 vector (BD Biosciences Clontech) and sequenced. Constructs expressing p140Cap domains were cloned as described: full-length p140Cap cDNA was digested with XhoI. A DNA fragment of 2310 bp and a fragment of 1100 bp, corresponding to p140Cap aa 1-770 and aa 770-1140, respectively, were obtained and cloned into the XhoI site of pCDNA3.1/Myc-Hys expression vector. p140Cap aa 219-477 was obtained by full-length p140Cap digestion with PstI and cloned into the PstI site of pCDNA3.1/Myc-Hys. p140Cap aa 351-691 was obtained by specific amplification from full-length mouse p140Cap. Forward primer was designed to incorporate a restriction site for NheI (1158 bp) (primer sequence: GCTGGCTAGCTGCAAT GGACTCCCCGCCT), reverse primer was designed to incorporate a restriction site for HindIII (2175 bp) (primer sequence: GCAGAAGC TTGACAGCAGTGGGCTG). The amplified region was cloned into pCDNA3.1/Myc-Hys expression vector (Thermo Fisher Scientific). p140Cap aa 667-866 was obtained by specific amplification from full-length mouse p140Cap. Forward primer was designed to incorporate a restriction site for XbaI (primer sequence: AGATCTCCTCGGC CAGCAGCACCCCTGCA), reverse primer was designed to incorporate a restriction site for HindIII (primer sequence: AAGCTTCTAAC CCTCATCCACTTGCCTTCG), and the amplified DNA was cloned into XbaI/HindIII sites of pCDNA3.1/Myc-Hys expression vector from the p-GEM vector. p140Cap aa 728-1217 was cloned into Nhe site of pCDNA3.1/Myc-Hys expression vector. p140Cap aa 1-770 GFP was obtained from the Myc tagged vector with the restriction site for EcoRI and was cloned into GFP-N2 vector. p140Cap 728-1217 GFP was obtained from the Myc tagged vector with the restriction enzymes Nhe/SalI and was cloned into GFP-N3 vector.

pCI-EGFP-GluN1 was obtained from Addgene (plasmid #45446) pCI EGFP-GluN2A was obtained from Addgene (plasmid #45445), pEGFP-GluN2B (Addgene #45447), and PSD95-Flag (plasmid #15463). GST-GluN2A (1049-1464), GST-GluN2A (1349-1464), and GST-GluN2A (1244-1389) C-terminal tail constructs were kindly provided by Professor Gardoni.

Cell lines. Human HEK293 cells and COS7 cells were obtained from American type Culture Collection. Cells were cultured in DMEM supplemented with 10% heat-inactivated FBS and penicillin/streptomycin (100 U/ml and100 g/ml, respectively).

Cell lines transfection. HEK293 cells were transfected by calcium phosphate precipitation; 15 μg of cDNA was used to transfect one 10 cm plate, and cell density was 50%-80% confluent on the day of transfection. cDNA was mixed with sterilized milliQ water and with 50 µl of $CaCl_2$ 2.5 M to a final volume of 500 µl. The mix was slowly dropwise added to 500 µl of HEPES buffered saline (HBS) by gently vortexing. 24 h after transfection, the medium was refreshed and the following day, the cells were harvested, and proteins were extracted.

COS7 cells were transfected with Lipofectamine LTX (Thermo Fisher Scientific). For each condition, 0.5 μg of cDNA (GFP-GluN2A, GFP-GuN2B, p140Cap-RFP, PSD95-Flag tagged) was diluted into 100 μl of DMEM antibiotic and serum-free 2 μl of Lipofectamine LTX was added into the above diluted DNA solution and incubated for 25 min at room temperature. The cells were incubated at 37°C for 36 h and then were fixed with ice-cold 100% methanol for 15 min at −20°C.

Primary mouse hippocampal neurons cultures. Hippocampal neurons were isolated from the hippocampus of E16-E17 pups derived from breeding of heterozygous mice ($p140Cap^{+/-}$ female with $p140Cap^{+/-}$ male). The dissociated cells were plated onto 20 mm glass coverslips coated with poly-L lysine (Sigma) at the density of 1×10^5 cells/coverslip and maintained in Neurobasal (Thermo Fisher Scientific) supplement with B27, antibiotics, 2 mM glutamine, and 2 mM glutamate. Cells were fixed with ice-cold methanol for 10 min at −20°C or with 4% PFA, 4% sucrose for 10 min at room temperature according to the experiment.

Hippocampal neurons transfection. Primary hippocampal neurons were transfected at DIV 14 with Lipofectamine 2000 (Thermo Fisher Scientific) with cDNA plasmid for p140Cap (aa 1-770) and p140Cap (aa 728-1217), both GFP tagged. For each coverslip, 1 μg of DNA was incubated with 2 μl of Lipofectamine 2000 in neurobasal antibiotics-free medium for 20 min at room temperature. DNA/Lipofectamine solution was directly added to each coverslip and incubated for 30 min at 37°C. Neurons were then washed with neurobasal medium, and conditioned medium was put back on coverslips. Neurons were fixed after 48 h from transfection with methanol for 10 min at −20°C.

Chemical LTP (c-LTP). c-LTP was induced as reported (Otmakhov et al., 2004; Franchini et al., 2019). Briefly, neurons were incubated in ACSF (125 mM NaCl, 25 mM KCl, 2 mM $CaCl_2$, 33 mM glucose, and 25 mM HEPES) + 1 mM $MgCl_2$ for 30 min at 37°C. c-LTP induction was performed in ACSF $MgCl_2$ free with 50 μM Forskolin (Tocris), 0.1 μM Rolipram (Tocris) and 100 μM Picrotoxin (Tocris) for 16 min. Unstimulated neurons were treated with DMSO in the same conditions. After stimulation neurons were incubated back in ACSF with $MgCl_2$ for 15 min and then were fixed with methanol. Stimulation control was performed by WB for the phosphorylation of GluR1 on Ser 845.

Immunofluorescence. Fixed COS7 cells transfected with RFP and/or GFP constructs were incubated for 30 min with blocking solution (PBS 5%, BSA, Sigma) and then with primary antibodies for 1 h at room temperature in PBS and then with AlexaFluor dye secondary antibodies for 1 h protected from light. Samples were rinsed several times in PBS and mounted on glass slides or with ProLong (Thermo Fisher Scientific) mounting medium.

Hippocampal neurons were incubated with blocking solution (5% goat serum, 5% BSA 0,1% Triton X-100) for 30 min. Primary antibodies were diluted in PBS 1% goat serum and incubated overnight in a humid chamber. AlexaFluor dye secondary antibodies were incubated for 1 h protected from light. Phalloidin-FITC or -647 and anti-p140Cap conjugated with Alexa647 were incubated with secondary antibodies. Neurons were mounted on glass slides with Mowiol. Samples were examined using Nikon ViCo Video Confocal Microscope equipped with a triple bandpass filter set (FITC, TRITC, DAPI) and SP5 confocal microscope Leica equipped with four excitation laser lines (405 Diode, Argon, DPSS561, HeNe633). Images were analyzed with ImageJ software. Colocalization in COS7 cells was performed with the plug-in JACoP and was expressed with Manders coefficients M1 and M2, which are proportional to the amount of fluorescence of the colocalizing pixels in each color channel. Colocalization in neurons dendrites was assessed by manual counting of colocalizing dots in selected ROIs. Gated-stimulated emission depletion (g-STED) confocal scanning microscopy and GM1 staining

For g-STED microscopy, neurons were plated on 0.17 mm glass coverslips (#1.5) coated with L-polylysine. After 16 d, mature neurons were incubated with cholera toxin subunit β-488 conjugated for 10 min at 4° C (concentration 1 μg/ml). Cells were washed in PBS, fixed in 4% PFA, 4% sucrose for 10 min at room temperature, and permeabilized in 0.1% Triton X-100 for 5 min. Neurons were incubated with anti GluN2A antibody overnight in a humid chamber and revealed by goat-anti rabbit AlexaFluor-555 secondary antibody (Invitrogen) in combination with phalloidin-647 to visualize DS heads.

To acquire super-resolved images, a Leica TCS SP8 g-STED 3× laser-scanning microscope equipped with an HC PL APO 100×/1.40 objective was used (Leica Microsystems). Fluorochromes and fluorescent proteins were excited at the optimal wavelength by means of 80 MHz pulsed white light laser (470-670 nm), allowing time gating of fluorescence lifetimes. For STED, the appropriate, 592 or 660 nm, depletion laser was used. Fluorescence channels were scanned sequentially, and emission was revealed by means of hybrid spectral detectors (HyD SP, Leica Microsystems). STED images were deconvolved to reduce noise using the adaptive method of the Lightning package, based on the Richardson-Lucy algorithm optimized for the Leica system.

Telencephalon extracts preparation. Telencephalon was quickly isolated from the total brain and immersed in liquid nitrogen to snap freeze. The samples were stored at −80°C for later use or kept on ice for immediate homogenization. The tissue was homogenized with an electric homogenizer in RIPA buffer (150 mM NaCl, 1.0% NP-40, 0.5% sodium deoxycholate, 0.1% sodium dodecyl sulfate, 50 mM Tris, pH 8.0, 5 mM EGTA) supplemented with protease inhibitor (Roche protease inhibitors 25×) and phosphatase inhibitors (1 mM PMSF, 1 mM $NaOv_3$, 1 mM NaF, and 2 mM DTT). The homogenates were centrifuged for 45 min at 13,000 rpm at 4°C. The supernatant was collected and protein concentration was determined using the Bio-Rad protein assay method (Bio-Rad).

Synaptosomes preparation. Synaptosomes were prepared from the telencephalon of WT and *p140Cap KO* mice. The tissues were immediately transferred in 8 ml of ice-cold synaptosomes buffer (0.32 M sucrose, 4 mM HEPES pH 7.3, 1 mM EGTA) containing a freshly added protease inhibitor (Roche) and phosphatase inhibitor cocktail. The tissue was homogenized with a Dounce glass homogenizer and glass pestle (Sigma Aldrich) and centrifuged at 1000 × *g* at 4°C for 10 min to remove the pelleted nuclear fraction (P1). The resulting supernatant (S1) was centrifuged at 12,500 × *g* for 20 min at 4°C (JA 25.50 Beckman rotor, Sorvall) to yield the crude synaptosome pellet (P2). S2 was discharged and P2 was resuspended in 10 ml of synaptosomes buffer and centrifuged again at 12,500 × *g* for another 20 min to yield the washed crude synaptosomal fraction. P2 was then resuspended in 2 ml of ice-cold lysis buffer (150 mM NaCl, 50 mM Tris, pH 7, 5% glycerol, 1% NP-40, 1 mM $MgCl_2$, protease and phosphatase inhibitors).

Synaptic NMDA receptor stimulation. For assessing NMDAR stimulation in synaptosomal preparations, we mimicked synaptic NMDAR activation according to Corera et al. (2009); 400 µg of P2 crude synaptosomes (see above) was suspended in physiological solution (125 mM NaCl, 26 mM $NaHCO_3$, 1.6 mM NaH_2PO_4, 2.5 mM $CaCl_2$, 5 mM KCl, pH 7.4, protease inhibitors), and left untreated or treated with 100 μM glycine for 20 min, at 37°C. Physiologic solution containing KCl at a 50 mM final concentration, was then added for 5-30 min. Samples were centrifuged at 12,500 × *g* for 20 min at 4°C, and the pellets were suspended in Triton insoluble fraction (TIF) buffer (1% Triton X-100, 20 mM HEPES, pH 7.4). TIF isolation was performed by ultracentrifugation for 1 h at 100,000 × *g* (SW70Ti; Beckman) at 4°C, and suspended in Laemmli 2×, before SDS-PAGE and WB analysis.

Immunoprecipitation (IP). IP was performed from HEK293 cell extracts and from WT and p140Cap KO crude synaptosomes in the lysis buffer (see above); 0.2 mg of Dynabeads protein G (30 mg Dynabeads/ml Thermo Fisher Scientific) was initially washed using PBS 1 × 0.02% Tween and then incubated with 1 µg antibody for 10 min at room temperature. The complex was washed PBS 1 × 0.02% Tween and incubated with 1 mg of extract for 2 h at 4°C. Beads were washed 5 times with cold lysis buffer, then resuspended in 10 µl of Laemmli buffer in reducing conditions, and incubated at 95°C for 10 min.

Western Blots (WB). WBs were performed with Mini-PROTEANR TGXTM Precast Gradient 4%-15% Gels from Bio-Rad (94547). Samples were mixed with Laemmli buffer (4× solution: SDS 8%, glycerol 40%, Tris-HCl, pH 6.8, 0.625 M phenol blue, 5% β-mercaptoethanol), boiled for 10 min at 95°C, and subjected to SDS-PAGE using Running Buffer (10× solution: 250 mM Tris, 1.92 M glycine, SDS 1%). Gels were transferred on nitrocellulose blotting membrane (GE Healthcare Life Sciences) with cold Towbin buffer (25 mM Tris, 192 mM glycine, 20% methanol). Membranes were blocked with TBS (50 mM Tris, pH 7.5, 150 mM NaCl) with 5% milk for 1 h at room temperature and incubated with primary antibodies diluted in TBS 1% BSA overnight at 4°C. Membranes were incubated with secondary antibodies for 1 h at room temperature and then developed with Bio-Rad's Clarity ECL on ChemiDoc Touch Imaging System.

Pull-down assays. Overnight cultures from single colonies of *Escherichia coli* transformed with the plasmid of GluN2A C-terminal tail (aa 1049-1464, aa 1349-1464, aa 1244-1389) all GST-tagged were grown overnight in 50 ml of Luria-Bertani medium containing 100 µg/ml ampicillin (Sigma) at 37°C. Bacterial suspension was refreshed by dilution with Luria-Bertani (1:10) under the same conditions for 2 h. Synthesis of recombinant proteins was induced by 0.1 mM isopropyl-L-D-thiogalactopyranoside (Sigma). The bacteria were grown for another 4 h and harvested by centrifugation. Bacterial pellets were resuspended with ice-cold PBS containing 5 mM DTT, 100 µg/ml lysozyme, 0.1 mM PMSF, and incubated on ice for 15 min. Lysis was achieved by the addition of 1.5% N-laurylsarcosine (Sarkosyl) from a 10% stock in PBS. Bacteria were sonicated on ice for 1 min, and the lysate was clarified by centrifuging at 10,000 × *g* (5 min, 4°C) in a JA 25.50 Beckman rotor (Sorvall).

Pull-down experiments, to evaluate the direct interaction between p140Cap and GluN2A, were performed using MBP-p140Cap (aa 261-730) and GST-GluN2A full carboxy terminal tail (aa 1049-1464) fusion proteins or GST alone as control. Glutathione Sepharose 4B Cytiva (17-0756-01 GE Healthcare Life Sciences) was washed with interaction buffer (50 mM Tris-HCl, pH 7.4, 150 mM NaCl, 1% Triton X-100) and then incubated with GST supernatants for 1 h at 4°C in interaction buffer. The complex was then washed 3 times and incubated with MBP-p140Cap protein for 1 h at 4°C. Following incubation, Sepharose was washed 7 times with the interaction buffer and resuspended in Laemmli buffer in reducing conditions for WB analysis.

Pull-down experiments to evaluate p140Cap interaction with different regions of GluN2A were performed by incubating GST-GluN2A supernatants (1049-1464, 1349-1464, and 1244-1389) with Glutathione Sepharose 4B in lysis buffer. Sepharose-bound proteins were washed 5 times with lysis buffer, and then were incubated with 1 mg of extract from WT crude synaptosomes or HEK293 cells stably expressing p140Cap-RFP for 2 h at 4°C. After incubation, the Sepharose was washed 10 times with the lysis buffer with 0.5% Triton X-100 and resuspended in the Laemmli buffer in reducing conditions for WB analysis.

Rac GTPases activity assay. For GST-PAK pull-down assay, 20 µg/sample of PAK-GST protein beads (Cytoskeleton) was used. The assay was performed using 2 mg of crude synaptosomal lysed in ice-cold lysis buffer. The extracts were incubated with PAK-GST beads for 1 h at 4°C under rotation. Beads were then centrifuged at 5200 × *g* (4°C) for 1 min, supernatant was discarded, and beads were washed twice in wash buffer (25 mM Tris, pH 7.5, 30 mM $MgCl_2$, 40 mM NaCl). Pellets were resuspended in 25 µl of Laemmli buffer in reducing conditions and analyzed in WB.

Patch-clamp experiments. Patch-clamp recordings were performed in whole-cell configuration using a Multiclamp 700-B amplifier connected to a Digidata 1440 and governed by the pClamp10 software (Molecular Devices). Patch electrodes, fabricated from thick borosilicate glasses (Hilgenberg), were pulled to a final resistance of 3-5 MΩ. Currents activated by NMDA administration (I_{NMDA}) were recorded in voltage-clamp conditions, holding neurons at –70 mV (V_h). Experiments were performed at room temperature (22°C-24°C) and acquired with sample frequency of 10 kHz. eEPSCs were filtered at half the acquisition rate with 8-pole low-pass Bessel filter. Recording with leak current >100 pA or series resistance >20 MΩ were discarded. Analysis was performed with Clampfit software (Molecular Devices).

Solutions and drugs. For voltage-clamp recordings, the external solution contained the following (in mM): 130 NaCl, 1.8 $CaCl_2$, 10 HEPES, 10 glucose, 1.2 glycine, pH 7.4. The internal solution contained the following (in mM): 90 CsCl, 8 NaCl, 20 TEACl, 10 EGTA, 10 glucose, 1 $MgCl_2$, 4 ATP, 0.5 GTP, 15 phosphocreatine, pH 7.4 with CsOH. For blocking synaptic currents because of the activation of glutamatergic AMPARs and GABAergic synapses ($GABA_A$ receptors), we added, respectively, DNQX (20 µM, Sigma-Aldrich) and picrotoxin (100 µM, Sigma-Aldrich). TTX (0.3 µM, Tocris Bioscience) was added to block voltage-gated Na^+ channels. The neuron was constantly superfused through a gravity system that allowed a rapid change (50-60 ms) of the solutions and the recording of I_{NMDA} following NMDA administration at different concentrations. During these experiments, NMDA was administered to neurons until I_{NMDA} reached the maximum amplitude.

LR isolation from total brain. LRs were purified as previously described in Delint-Ramirez et al. (2010) with some modifications. The telencephalon was homogenized in LR buffer (0.5 ml of 150 mM NaCl, 25 mM Tris-Cl buffer, pH 7.5, containing 50 mM NaF, 10 mM NaP_2O_7, 1 mM sodium orthovanadate, complete protease inhibitors cocktail) and 1% Triton X-100; 2 mg Triton X-100 extracts were incubated for 30 min at 4°C and centrifuged (13,000 × *g*, 4°C, 10 min) to separate the detergent-insoluble pellet. Triton X-100-insoluble pellet was resuspended in 0.5 ml of lysis buffer and mixed with 1 ml sucrose 2 M, overlaid with 2 ml of sucrose 1 M, and with 1.5 ml of sucrose 0.2 M. The gradient was centrifuged for 18 h at 200,000 × *g* (SW40Ti; Beckman) at 4°C. After centrifugation, 1.1 ml fractions were collected from the top to the bottom of the gradient. Equal volumes of each fraction were subjected to WB analysis.

Synaptic LR isolation. Synaptic LRs were prepared from crude synaptosomal pellets (P2); 4 mg of P2 was resuspended with 1 ml of LR buffer (see above) containing 1% Triton X-100 and incubated for 30 min at 4°C. The suspension was then mixed with 1 ml of sucrose 90% to achieve a final sucrose percentage of 45%. The gradient was completed with 4 ml of sucrose 35% and 4 ml of sucrose 5%, and it was centrifuged at 200,000 × *g* for 18 h at 4°C (SW 40 Ti; Beckman). After centrifugation, 1.1 ml fractions were collected from the top to the bottom of the gradient. Equal volumes of each fraction were subjected to WB analysis.

Dot blot for GM1. The level of enrichment of monosialoganglioside (GM1) was determined as described by Delint-Ramirez et al. (2010) with some modification. Briefly, 1 µl of each density gradient fraction was dot blotted onto nitrocellulose, and membrane was saturated with TBS 5% BSA for 2 h. After incubation with HRP-conjugated cholera toxin B (1/20,000) (Sigma), the dots were revealed by chemiluminescence.

Statistical analysis. All statistical analysis was performed with Prism GraphPad (version 8.0.1). "*n*" indicates the number of biological replicates for each experiment as indicated in each figure legend. To compare one variable, the two-tailed paired Student's *t* test was performed. All bar graphs are represented as mean ± SEM.

Results

p140Cap is a new interaction partner of the GluN2A subunit of the NMDAR

Here we demonstrated that p140Cap coimmunoprecipitated with the NMDAR subunits GluN1, GluN2A, and GluN2B in mouse synaptosomes (Alfieri et al., 2017) (Fig. 1*A*). We further investigated the specificity of the p140Cap interaction with the different NMDAR subunits by coimmunoprecipitation experiments in

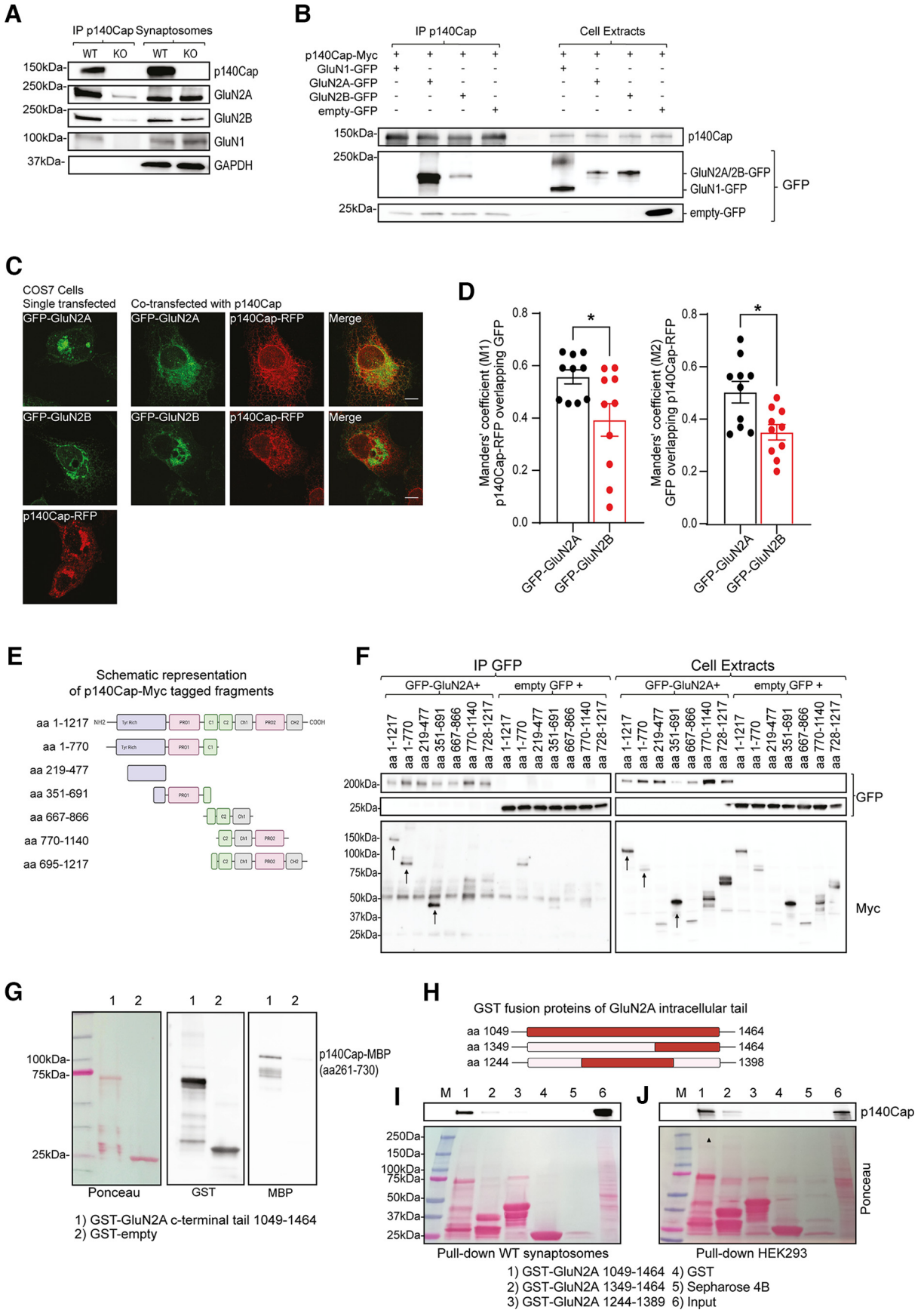

Figure 1. p140Cap directly interacts with GluN2A. ***A***, p140Cap IP and immunoblotting from 1 mg P2 fraction of crude synaptosomes. p140Cap KO synaptosomes were used as negative control; 30 μg synaptosome was loaded for each sample as loading control. ***B***, p140Cap IP and immunoblotting from 1 mg extracts from HEK293 cells cotransfected with Myc-tagged p140Cap and GFP-tagged NMDAR subunit GluN1, GluN2A, GluN2B, or empty-GFP as negative control; 30 μg extracts were loaded for each sample as loading control. ***C***, ***D***, Confocal imaging of COS-7

heterologous cells. To this end, cell extracts from HEK293 cells cotransfected with Myc-tagged p140Cap cDNA in combination with GFP-tagged GluN1, GluN2A, and GluN2B subunit constructs were immunoprecipitated with anti-p140Cap antibody and were analyzed by WB with anti-GFP antibody. p140Cap was specifically associated with the GluN2A subunit (Fig. 1*B*); conversely, the association was weaker with GluN2B and totally absent with GluN1 (Fig. 1*B*). Accordingly, immunofluorescence experiments performed in COS7 cells cotransfected with p140Cap in combination with GluN2A and GluN2B subunits showed a significant higher colocalization between p140Cap and GluN2A compared with GluN2B (Fig. 1*C*,*D*) (in Fig. 1*D*: M1 $p = 0.0453$, M2 $p = 0.0264$, paired t test). Interestingly, both GluN2A and GluN2B subunits transfected alone displayed a perinuclear distribution (Gardoni et al., 2003; Stanic et al., 2015). However, GluN2A underwent redistribution throughout the cell when it was coexpressed with p140Cap, while GluN2B perinuclear localization was not affected (Fig. 1*C*), further confirming that p140Cap mainly associates with the GluN2A subunit and has an impact on its subcellular localization.

To identify the binding regions involved in the association, a panel of Myc-tagged p140Cap fragments (Chapelle et al., 2020) represented in Figure 1*E* were cotransfected with GFP-GluN2A or with empty GFP vectors as negative control in HEK293 cells. The IP with anti-GFP antibody pointed out that both the p140Cap N-terminal region (aa 1-770) and the proline-rich region 1 encoded by aa 351-691 can associate with GluN2A (Fig. 1*F*). To assess direct physical interaction between GluN2A and p140Cap, Glutathione S-transferase (GST) pull-down assay was performed. The recombinant GST-GluN2A fusion protein (aa 1049-1464), corresponding to the full intracellular C-terminal tail (Fig. 1*G*) or the GST protein, as negative control, were immobilized on Glutathione Sepharose 4B beads. The beads were then incubated with a p140Cap-MBP fragment including the proline-rich domain 1 (aa 261-730). WB with anti-MBP antibody revealed the direct binding between p140Cap and GluN2A recombinant proteins (Fig. 1*G*). To identify the GluN2A region responsible for the interaction with p140Cap, GST fusion proteins for GluN2A full intracellular domain (aa 1049-1464), and for two enclosed regions (aa 1349-1461 and aa 1244-1389) (Fig. 1*H*) were immobilized on Glutathione Sepharose 4B beads. Both in mouse synaptosomes extracts (Fig. 1*I*) or in HEK293 cell extracts stably expressing p140Cap-RFP (Fig. 1*J*), the GluN2A region 1349-1464 was sufficient for the interaction with p140Cap. However, the binding of this small fragment was weaker than that obtained with the large fragment 1049-1464, suggesting that the entire C-terminal tail of GluN2A owns the optimal conformation for the interaction with p140Cap. Overall, these results provide the first evidence that p140Cap is a direct binding partner of the GluN2A subunit of NMDAR.

The association between p140Cap and GluN2A occurs during synaptogenesis, increases on c-LTP induction, and is required for NMDAR-dependent LTP

Based on the results shown above, we wondered whether p140Cap could influence GluN2A temporal expression. However, in hippocampal neurons and in telencephalon extracts from WT and *p140Cap KO* mice, GluN2A temporal expression and protein level were not affected by p140Cap as shown in Figure 2*A* and Figure 2*B*, respectively. To investigate the association between p140Cap and GluN2A-associated proteins during brain development, we analyzed WT telencephalon at different postnatal days (P0, P7, P14, P21, P60) (Fig. 2*C*). WB analysis of telencephalon extracts showed that p140Cap is present from P0, consistently with previous works (Ito et al., 2008), and its expression increased at P7 and remained constant afterward. By contrast, GluN2A and PSD95 are expressed later, as previously shown (Gonzalez-Lozano et al., 2016). IP experiments with p140Cap antibody revealed that the association with the GluN2A-PSD95 complex was quantitatively relevant only from P14 (Fig. 2*C*). Interestingly, also Flotillin-1, which is expressed from P0, was immunoprecipitated with p140Cap only at P14, suggesting that the formation of the complex is strictly time-dependent during development, requiring a precise subcellular localization of the different components. Coherently, GluN2A IP from telencephalon at the selected time points P7, P10, and P14, confirmed that GluN2A can associate with its partners only from P14 (Fig. 2*D*). Since P14 corresponds to the peak of synaptogenesis (Gonzalez-Lozano et al., 2016), these results suggest that the formation of the complex occurs during synapse development. To further investigate the dynamic of the p140Cap/GluN2A complex formation also at cellular level, we performed immunofluorescence for GluN2A and p140Cap in neurons at selected time points (DIV 10, 14, 17) in which both p140Cap and GluN2A are expressed (Fig. 2*E*). Indeed, GluN2A expression is known to increase during hippocampal neuron maturation, and it starts to be expressed from DIV 5 (Siow et al., 2010) while p140Cap is already expressed at DIV 0 (Fig. 2*C*). At DIV 10, p140Cap was already well expressed while GluN2A staining was weaker, and the two molecules did not colocalize. In contrast, p140Cap and GluN2A colocalization was clearly detectable at DIV14 and further increased at DIV 17 (Fig. 2*E*), suggesting that the association can occur only in late phases of neuron maturation and likely depends on synaptic activity.

To test this hypothesis, we investigated whether synaptic remodeling, which occurs during LTP, could modulate the complex. To this end, we treated hippocampal neurons at DIV 16 with a forskolin/rolipram/picrotoxin cocktail to induce c-LTP (Otmakhov et al., 2004; Franchini et al., 2019). Proper c-LTP stimulation was validated by WB analysis of mature neuron extracts to detect the increased Ser845 phosphorylation in the GluR1 subunit of the AMPAR (Esteban, 2003; Oh et al., 2006; Hu et al., 2007; Makino et al., 2011) (Fig. 3*A*,*B*). We found a significant increase of p140Cap colocalization with the presynaptic marker Bassoon, demonstrating an increased p140Cap recruitment to the DSs on c-LTP (Fig. 3*C*,*D*) (in Fig. 3*D*, $p = 0.0015$

←

cells cotransfected with p140Cap-RFP (red) in combination with GFP-GluN2A (green) or GFP-GluN2B (green). The GFP signal was enhanced with anti-GFP mAb. Scale bar, 12 μm. ***D***, Manders' overlap coefficients are represented as the average of $n = 10$ individual cell quantification M1 $p = 0.0453$, M2 $p = 0.0264$, paired t test. ***E***, Schematic representation of Myc-tagged p140Cap fragments. ***F***, GFP IP and immunoblotting from 1 mg extracts from HEK293 cells cotransfected with the constructs shown in ***E*** together with GFP-GluN2A. Empty GFP in combination with p140Cap fragments was used as negative control; 30 μg extracts were loaded for each sample as loading control. ***G***, GST pull-down assay with a Sepharose 4B column charged with the C-terminal GST-GluN2A fusion protein (aa 1049-1464), incubated with the p140Cap-MBP fusion protein (aa 261-730). Empty GST was used as negative control. Immunoblot with antibodies to MBP to reveal p140Cap binding (right), to GST as control of GST binding to the column (middle), and Ponceau staining as loading control. ***H***, Schematic representation of C-terminal GST-GluN2A recombinant proteins. ***I***, p140Cap immunoblotting of pull-down assay from columns of GST-GluN2A fragments incubated with 1 mg WT synaptosomes. Empty-GST and Sepharose 4B beads were used as negative controls. ***J***, GST pull-down assay with a Sepharose 4B column charged with GST-GluN2A fragments incubated with 1 mg cell extracts from HEK293 cells stably expressing p140Cap-RFP.

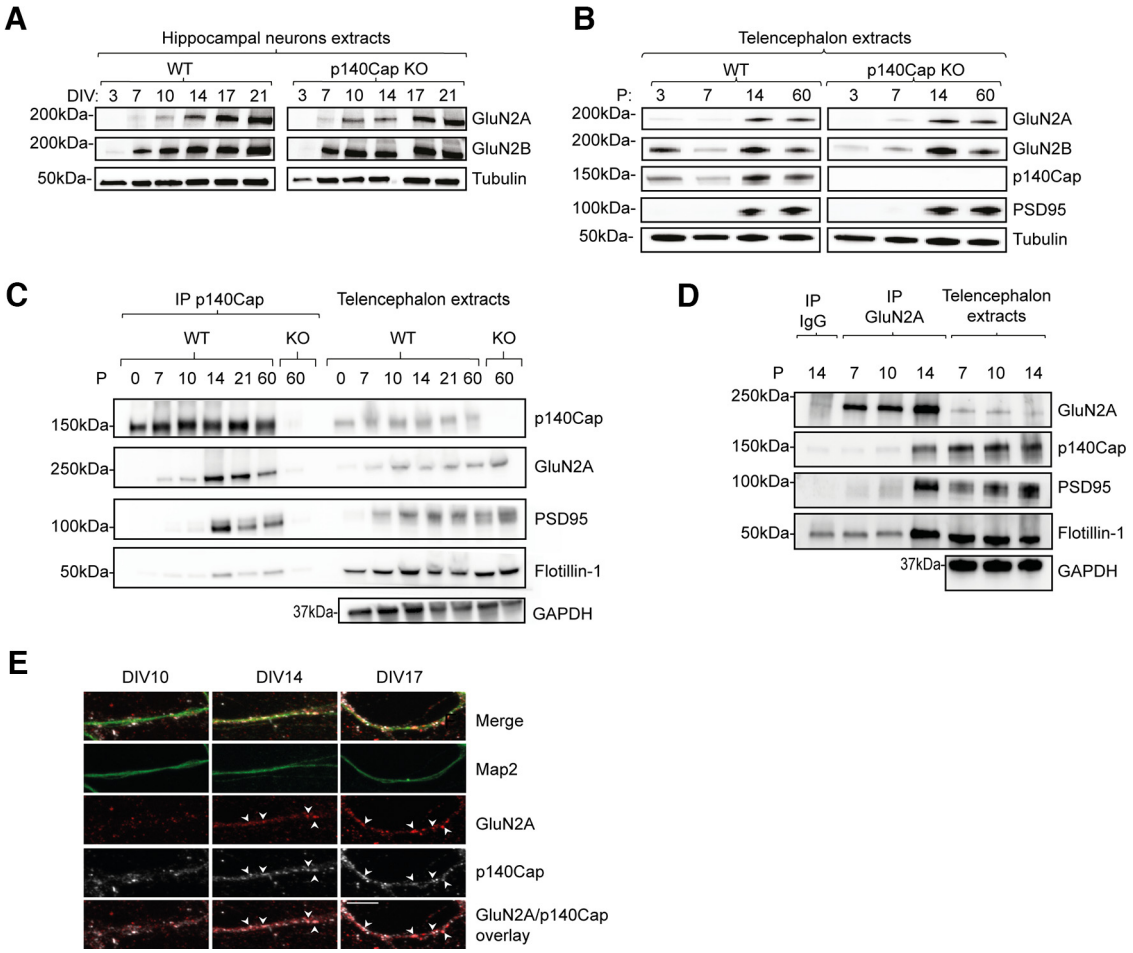

Figure 2. Kinetics of p140Cap and GluN2A complex formation during brain development. ***A***, WT and *p140Cap KO* hippocampal neuron extracts at different DIV (3, 7, 10, 14, 17, and 21) were immunoblotted with indicated antibodies; 30 μg was loaded for each time point. Tubulin was used as loading control. ***B***, Telencephalon extracts from WT and *p140Cap KO* mice at different postnatal days (P) (P0, P7, P14, P60) were immunoblotted with the indicated antibodies; 50 μg of extracts was loaded for IP control. Tubulin was used as loading control. ***C***, p140Cap IP and immunoblotting from 1 mg telencephalon extracts at the indicated postnatal days (P). IP with *p140Cap KO* P60 telencephalon was used as negative control; 30 μg of extracts was loaded as IP control. GAPDH was used as loading control. ***D***, GluN2A IP and immunoblotting from telencephalon extracts (1 mg) at selected postnatal days. Mock rabbit IgGs were used in P14 telencephalon as negative control; 30 μg of extract was loaded for IP control. GAPDH was used as loading control. ***E***, GluN2A, p140Cap, and Map2 immunofluorescence in WT hippocampal neurons at indicated DIV. Neurons were fixed with 4% PFA 4% sucrose. Scale bars: 5 μm; segment length, 20 μm.

paired *t* test). Moreover, GluN2A and p140Cap fluorescent immunolabeling analysis revealed a significant increase in protein colocalization on c-LTP stimulation (Fig. 3*E*,*F*) (in Fig. 3*F*, $p = 0.0049$ paired *t* test), suggesting that the formation of the p140Cap-GluN2A molecular complex increases on LTP stimulation.

We next asked whether the GluN2A/p140Cap association merely regulates NMDAR-dependent LTP. Previous work showed that the activity-dependent stimulation of synaptic NMDARs can regulate the insertion of AMPARs into postsynaptic sites, thus inducing LTP (Bredt and Nicoll, 2003). In particular, Corera et al. (2009) have shown in synaptosomes that application of glycine (a NMDAR co-agonist) results in the pre-activation of synaptic NMDARs; next, NMDARs can be fully activated by KCl-dependent depolarization, which promotes glutamate release from presynaptic terminals. This leads to a rapid surface increase of AMPARs into synaptic sites, which is prevented by blocking NMDARs with AP5. In synaptosomes from WT adult mice, we found that treatment with glycine alone did not alter the level of GluR1 in the TIF, while KCl stimulation induced a strong increase in GluR1 in the same compartment (Fig. 3*G*). Moreover, the GluR1 increase in TIF was completely abolished in the *p140Cap KO* (Fig. 3*G*), suggesting that p140Cap is required to regulate NMDAR-dependent LTP.

Overall, these data indicate that both *ex vivo* and *in vitro*, the formation of the p140Cap and GluN2A-containing NMDAR molecular complex is time-dependent, requires the recruitment of specific DS components, and is necessary for physiological NMDAR-dependent LTP (Fig. 3*G*). This mechanism could underlie the impairment of NMDAR-dependent LTP that we observed in p140Cap KO mice (Repetto et al., 2014).

p140Cap controls the composition of the molecular complex associated to GluN2A-containing NMDARs

In DSs, the NMDAR GluN2A subunit is associated with a large multiprotein complex, which includes scaffold proteins (PSD95, Homer1) (Husi et al., 2000; Shiraishi et al., 2003), signaling proteins (Groveman et al., 2012), molecules involved in NMDAR recruitment into LRs (Flotillin-1) (Swanwick et al., 2009), and molecules involved in actin dynamics, such as the small GTPase Rac1 (Swanwick et al., 2009).

By IP of p140Cap from P2 crude synaptosomes, we found that PSD95, Rac1, and Flotillin-1 also associated with p140Cap.

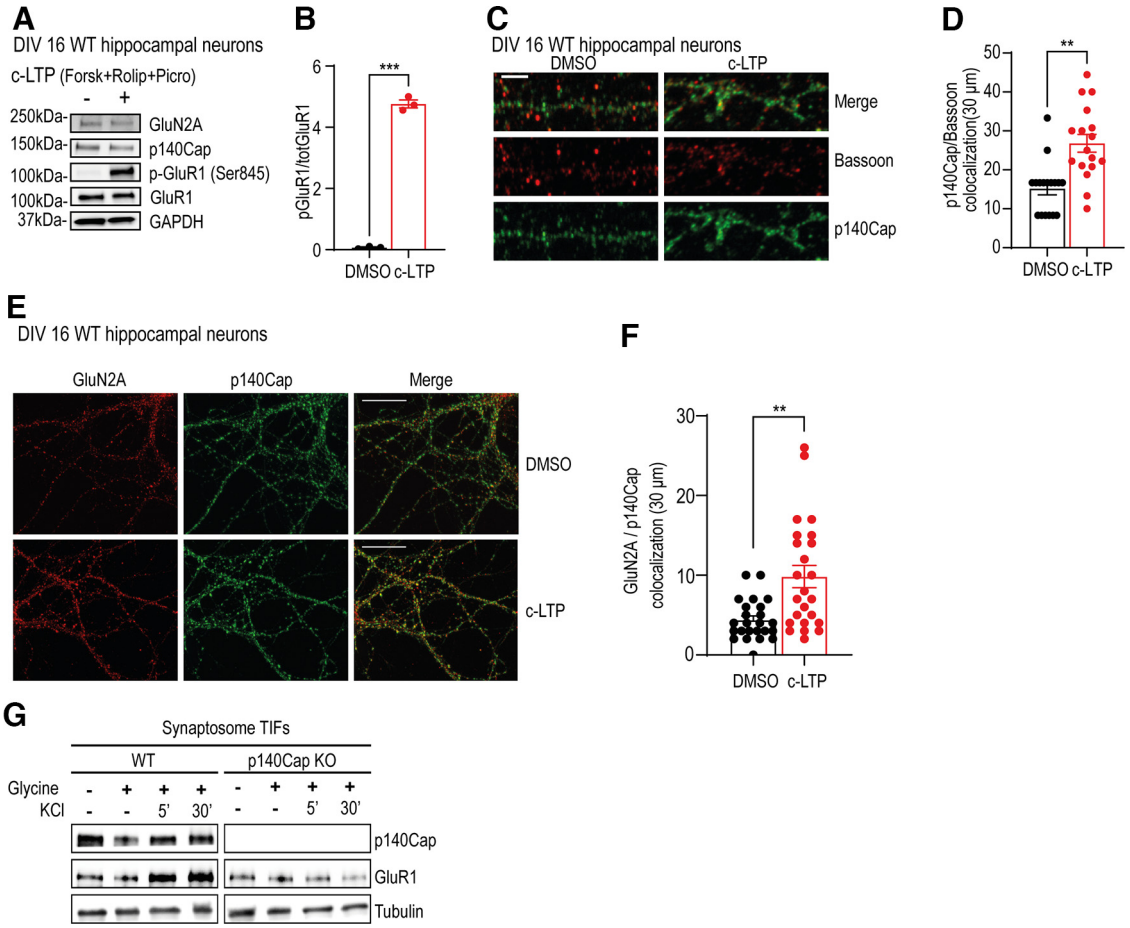

Figure 3. p140Cap and GluN2A complex formation on c-LTP induction and NMDAR-dependent LTP. ***A***, 30 µg of extracts from DIV 16 WT hippocampal neuron extracts on DMSO or c-LTP treatment was loaded and immunoblotted with antibodies to phosphorylated GluR1 subunit of the AMPAR (pGluR1 Ser845). ***B***, The ratio of p-GluR1 on total GluR1 is shown from $n = 3$ independent experiments ($p = 0.001$, paired t test). ***C***, p140Cap and Bassoon colocalization in DIV 16 hippocampal neurons on DMSO or c-LTP treatment. Scale bar, 5 μm. ***D***, Quantification for colocalization obtained from the analysis of 30 μm; $n = 17$ for each experimental group ($p = 0.0015$, paired t test). ***E***, p140Cap and GluN2A colocalization in DIV 16 hippocampal neurons on DMSO or c-LTP treatment. Neurons were fixed with methanol. Scale bar, 20 μm. ***F***, Quantification of colocalization obtained from the analysis of 30 μm segments; $n = 24$ for each experimental group ($p = 0.0049$, paired t test). ***G***, Immunoblot analysis of TIF prepared from xx WT and *p140Cap KO* synaptosomes, left untreated or on stimulation with glycine and KCl for the indicated times; 20 μg of extracts was loaded for each condition. Tubulin was used as loading control.

Interestingly, no association was found with Cdc42, another Rho GTPase protein (Fig. 4*A*). To investigate whether p140Cap could influence the composition of the molecular complex associated to GluN2A-containing NMDAR at the post synapse, we compared the composition of GluN2A-associated molecular complex in synaptosomes isolated from WT and from *p140Cap KO* adult mice (Fig. 4*B*). Total protein levels were unaffected between the two genotypes; however, in *p140Cap KO* synaptosomes, GluN2A was significantly less associated to PSD95, Flotillin-1, and Rac1 than in WT synaptosomes (Fig. 4*C–E*): paired t test for Figure 4*C* (PSD95) $p = 0.0157$, for Figure 4*D* (Rac1) $p = 0.0065$, and for Figure 4*E* (Flotillin-1) $p = 0.0293$. By contrast, GluN2A association with other proteins as Tiam1 was similar between the genotypes (Fig. 4*F*). These data suggest a specific role of p140Cap in the recruitment of PSD95, Rac1, and Flotillin-1 in the GluN2A-associated molecular complexes. Moreover, we also checked for Rac1 activity by performing GST-PAK pull-down assay on synaptosomes. As shown in Figure 4*G*, *H*, we found a significant decrease of Rac1 activity in *p140Cap KO* synaptosomes compared with WT (in Fig. 4*H*: paired t test $p = 0.0047$), suggesting the relevance of p140Cap not only for Rac1 recruitment to NMDAR molecular complex but also for its activation.

These data underline that p140Cap can influence the composition of the GluN2A-containing NMDAR complex and its functional activity, in terms of Rac1 activation

In *p140Cap KO* neurons, the current mediated by activation of single NMDAR is reduced. In addition to the biochemical analysis, to assess whether the presence of p140Cap may regulate the activity of NMDARs, we acutely administered NMDA at different concentrations on cultured hippocampal neurons, to study both synaptic and extrasynaptic NMDARs (Harris and Pettit, 2007) by avoiding any possible presynaptic effect produced by the loss of p140Cap (Russo et al., 2019). We therefore performed patch-clamp experiments and measured currents mediated by NMDARs in hippocampal neurons at DIV 16. The experiments, performed by holding neurons at $V_h = -70$ mV, showed that NMDA administered at concentrations comprised between 6 and 300 μM induces a mean inward current (I_{NMDA}) not significantly different in WT ($n = 16$) and *KO* ($n = 19$) neurons. In particular, the current activated by 6, 10, 50, and 300 μM of NMDA was, respectively, 86.5 ± 19.0 pA in WT and 99.5 ± 15.1 pA in *KO*, 159.2 ± 34.6 pA in WT and 194.7 ± 20.1 pA in *KO*, 440.9 ± 68.8 pA in WT and 554.7 ± 89.9 pA in *KO*, 592.4 ± 89.3 pA in WT and 854.9 ± 112.4 pA in *KO* neurons (Fig. 5*A–C*). Plots of normalized NMDA current (I_{NMDA}) versus NMDA concentration

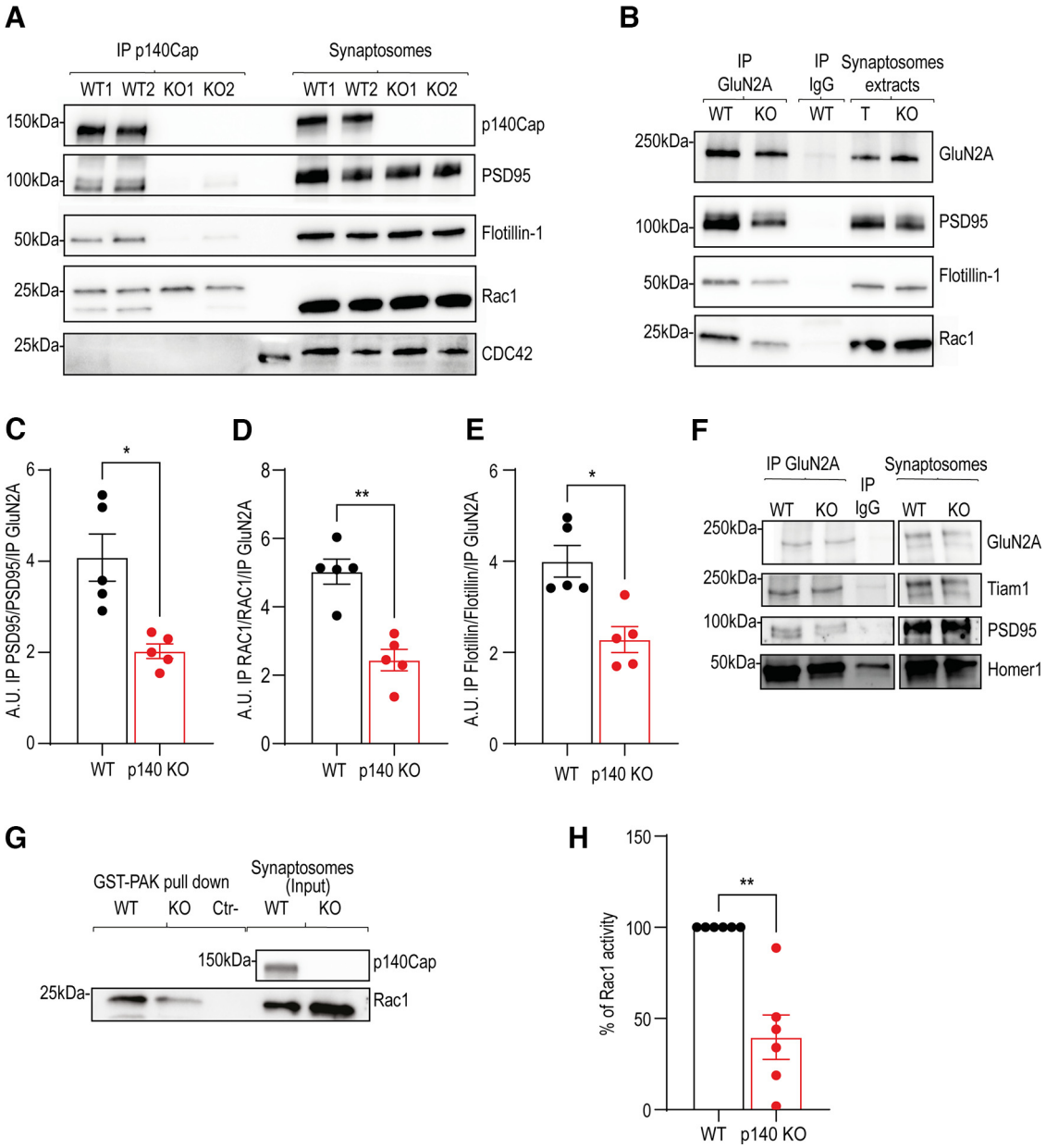

Figure 4. Composition of GluN2A-associated molecular complexes in WT and *p140Cap KO* synaptosomes. ***A***, p140Cap IP and immunoblotting from 1 mg P2 fraction of crude synaptosomes. p140Cap KO synaptosomes were used as negative control. ***B-E***, GluN2A IP and immunoblotting from 1 mg WT and *p140Cap KO* adult mice P2 fraction of crude synaptosomes. Mock rabbit IgG was used in WT synaptosomes as negative control. ***C-E***, The quantification of the coimmunoprecipitation is expressed as arbitrary units (A.U.) calculated as follows: the ratio of coimmunoprecipitation on the corresponding input (synaptosomes) and on the IP protein (GluN2A). Data are representative from $n = 5$ mice per experimental group, paired *t* test for ***C*** (PSD95) $p = 0.0157$, for ***D*** (Rac1) $p = 0.0065$, and for ***E*** (Flotillin-1) $p = 0.0293$. ***F***, GluN2A IP and immunoblotting from 1 mg WT and *p140Cap KO* adult mice P2 fraction of crude synaptosomes. Tiam1 antibodies were used as negative control. Mock rabbit IgG were used in WT synaptosomes as negative control of the IP. ***G***, GST-PAK pull-down for Rac1 activity on WT and *p140Cap KO* adult mice P2 fraction of crude synaptosomes; 2 mg was used for the assay while 30 μg was loaded as input. ***H***, Data are presented as the percentage of Rac1 activation in $n = 6$ independent preparations of synaptosomes for each genotype ($p = 0.0047$ paired *t* test).

exhibited dose–response relationships fitted by the Hill equation $Y = I_{max}\frac{x^n}{k^n + x^n}$ of similar steepness (n) (0.9 ± 0.2 in WT vs 0.9 ± 0.1 in KO) and EC_{50} (k) (28.1 ± 8.3 in WT vs 30.1 ± 8.9 in KO) (Fig. 4*D*). We thus concluded that, in *KO* neurons, I_{NMDA} amplitude is comparable to that measured in WT and that the stoichiometry as well as the ligand-receptor binding affinity is not altered in KO cells. When traces of I_{NMDA} activated by 300 μM were observed at higher magnitude, we noticed increased and more discrete fluctuations in WT than in *KO* neurons (Fig. 5*E*,*F*). Because differences in noise signal can be quantified by considering the variance (σ^2), we estimated the mean number of functioning NMDARs and their single-channel conductance both in WT and in *KO* neurons, by comparing σ^2 of I_{NMDA} (Sigworth, 1980). We calculated σ^2 for periods of 2 s during stationary conditions of I_{NMDA} and plotted the values as a function of the average I_{NMDA} amplitudes generated by increased NMDA concentration (Traynelis and Jaramillo, 1998). The relationship between σ^2 and I_{NMDA} is described by the following parabolic equation: $\sigma^2 = iI - I^2/n$, where i is the unitary current of NMDARs, n the number of activated NMDARs, and I the mean I_{NMDA} amplitude (Fig. 5*G*,*H*). The

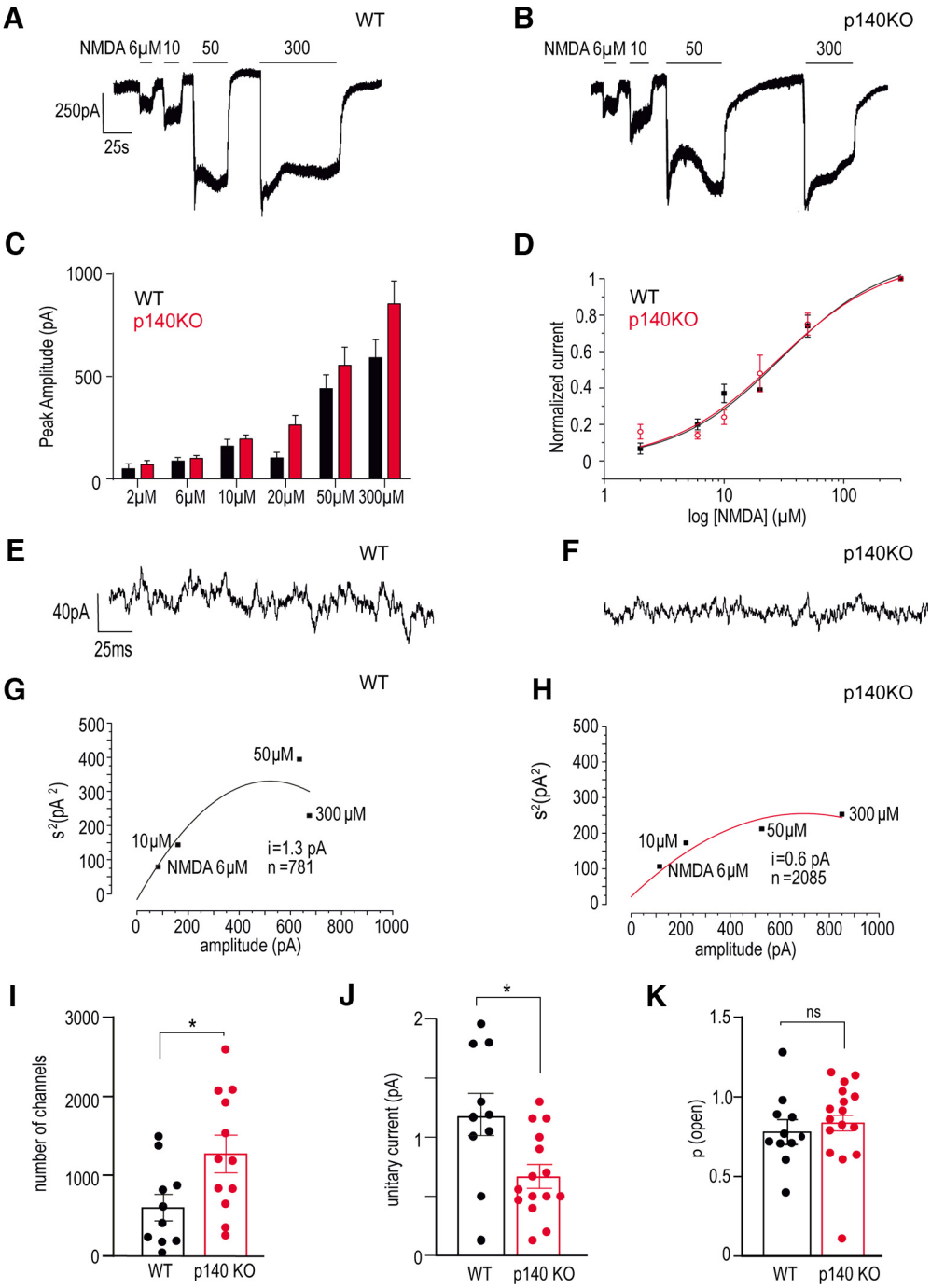

Figure 5. Electrophysiological properties of NMDARs in *p140Cap KO* neurons. ***A-C***, Representative inward currents activated by increasing concentrations of NMDA (from 6 to 300 μM), respectively, in WT (***A***) and *p140Cap KO* neurons (***B***). ***C***, Bar graph summarizing the average amplitude of inward currents activated by NMDA. ***D***, The dose–response sigmoid curve of the current activated by NMDA (from 62 to 300 μM) is not affected by p140Cap. ***E***, ***F***, Inward currents of 2 s duration activated by 300 μM of NMDA shown at expanded scale showing the increased noise observed in WT (***E***) compared with *p140Cap KO* neurons (***F***). ***G***, ***H***, Representative parabolic relationship between the variance ($\sigma 2$) of noise signal and mean of the inward current activated by NMDA at different concentrations in WT (***G***) and *p140Cap KO* (***H***) neurons. ***I***, ***J***, ***K***, Bar graph sum marizing the significant increase of the average number of NMDARs induced in *p140Cap KO* neurons (***I***) and decrease of their unitary current (***J***), despite the open probability (***K***) remains unchanged. $*p < 0.05$ paired *t* test.

fit with the above parabolic function gave a number of NMDARs (n) that increased significantly in *KO* neurons (from 622.1 ± 173.6 in WT to 1302.2 ± 228.2 in *KO*; $*p < 0.05$ Student's *t* test) (Fig. 5*I*), despite a significant decrease of the single-channel unitary current (1) was observed (1.2 ± 0.2 pA in WT and 0.7 ± 0.1 pA in *KO*; $*p < 0.05$ Student's *t* test) (Fig. 5*J*). Finally, we estimated the maximum open probability of NMDAR channels $p = I/(N*i)$ (Traynelis and Jaramillo, 1998) where I is the maximum I_{NMDA} and found no significant changes between WT (0.79 ± 0.07) and *KO* neurons (0.84 ± 0.07) (Fig. 5*K*). These results show that the absence p140Cap modifies the intrinsic functional properties of NMDA receptors as well as their expression on membrane surface, leaving unaltered the average I_{NMDA} generated by activation of both synaptic and extrasynaptic NMDA receptors.

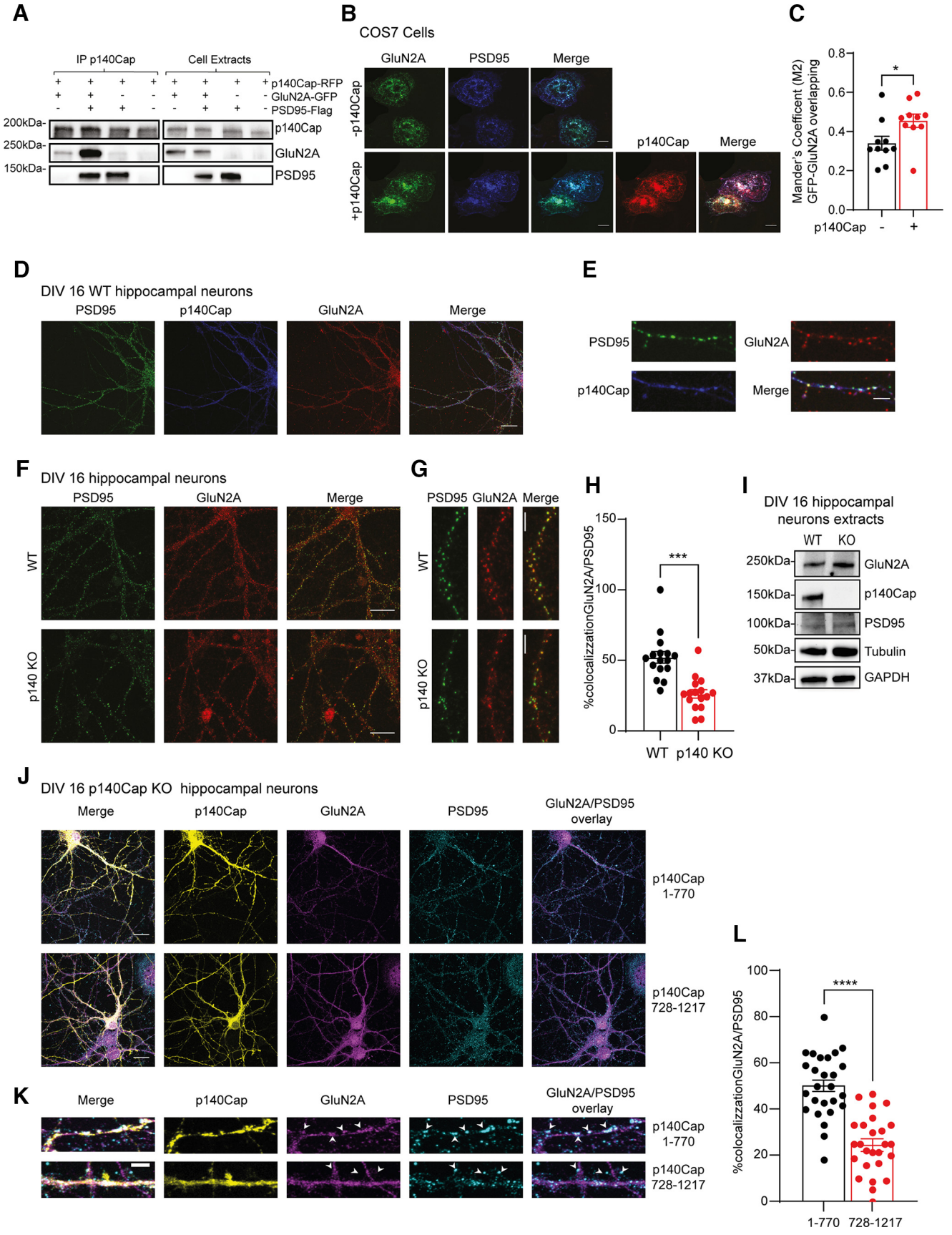

Figure 6. p140Cap potentiates GluN2A and PSD95 association in neurons and in heterologous cells. ***A***, p140Cap IP and immunoblotting from 1 mg extracts of HEK293 cells cotransfected with p140Cap-RFP and GFP-GluN2A or PSD95-Flag or both. ***B***, ***C***. PSD95-Flag and GFP-GluN2A clustering on transfection in COS-7 cells with or without p140Cap-RFP. Scale bar, 10 μm. ***C***, Manders' overlap coefficients for PSD95-Flag and GFP-GluN2A are represented as the average of $n = 10$ individual cell quantification ($p = 0.0369$, paired t test). ***D***, ***E***, GluN2A, PSD95, and p140Cap immunostaining performed on WT DIV 16 hippocampal neurons. Neurons were fixed with 4% PFA 4% sucrose. Staining for p140Cap was performed with α-p140Cap-647-conjugated

p140Cap potentiates the association between PSD95 and GluN2A

As is well known, PSD95 binds to the GluN2A C-terminal tail, thus stabilizing NMDAR at the cell surface and clustering GluN2 subunits in heterologous cells (Niethammer et al., 1996; Sheng and Kim, 2011). Our biochemical data revealed a reduced association of GluN2A with PSD95 in *p140Cap KO* synaptosomes (Fig. 4*B*), suggesting that p140Cap could potentiate or stabilize the PSD95/GluN2A partnership. Following this lead, we next demonstrated that p140Cap can associate with GluN2A and PSD95 independently, by coimmunoprecipitation analysis in HEK293 cells (Fig. 6*A*). Subsequently, we found that p140Cap could influence PSD95 and GluN2A clustering in heterologous COS7 cells and in WT DIV 16 hippocampal neurons. Coexpression of PSD95 with GluN2A in COS7 cells induced a significant GluN2A redistribution and the formation of plaque-like clusters as already described (Kim et al., 1996; Stanic et al., 2015) (Fig. 6*B*,*C*; Fig. 6*C*: $p = 0.0369$ paired *t* test). In cells triple-transfected with GluN2A, PSD95, and p140Cap, the formation of GluN2A-PSD95 clusters significantly increased. Moreover, the three proteins colocalized, indicating that p140Cap may take part of a ternary complex, including PSD95 and GluN2A, likely potentiating the association of PSD95 with GluN2A (Fig. 4*A*,*B*). Coherently, PSD95, GluN2A, and p140Cap also colocalized in DIV 16 WT hippocampal neurons (Fig. 6*D* and magnified in Fig. 6*E*).

To assess the role of p140Cap in the association between PSD95 and GluN2A, we took advantage of the hippocampal neurons isolated from *p140Cap KO* mice. We already know that *p140Cap KO* neurons have reduced numbers of mushroom spines (Repetto et al., 2014) and display reduced density of PSD95 puncta (Tomasoni et al., 2013). However, we here show that also the percentage of colocalization between GluN2A and PSD95 was significantly reduced in *p140Cap KO* neurons, suggesting that p140Cap can potentiate or stabilize the association between GluN2A and PSD95 (Fig. 6*F–H*) (in Fig. 6*H*: $p < 0.0001$ paired *t* test). Because the GluN2A and PSD95 protein levels did not grossly change between primary WT and *p140Cap KO* hippocampal neurons extracts (Fig. 6*I*), the reduced protein colocalization is unlikely to be because of decreased protein expression in the *p140Cap KO* neurons, but can be mainly attributed to a different localization. To further prove the role of p140Cap in stabilizing PSD95 and GluN2A association, we performed rescue experiments by transfecting *p140Cap KO* hippocampal neurons with cDNA constructs encoding either (1) the region aa 1-770 of p140Cap, which corresponds to the domain involved in GluN2A binding (see above Fig. 1*E*), or (2) the C-terminal region of p140Cap (aa 728-1217), which is instead not involved in the association (Fig. 6*J*,*K*). Immunofluorescence analysis revealed that p140Cap aa1-770 can rescue the percentage of GluN2A and PSD95 colocalization to the level of WT neurons, while p140Cap (aa 728-1217) has no effect on PSD95/GluN2A colocalization (Fig. 6*L*, $p < 0.0001$ paired *t* test). Overall, these results demonstrated that the p140Cap region required for the interaction with GluN2A is sufficient to potentiate the association between PSD95 and GluN2A.

Synaptic LRs from p140Cap KO mice contain reduced amounts of GluN2A and PSD95

The above data show that p140Cap may influence the composition of the molecular complex associated to GluN2A-containing NMDAR, indicating that p140Cap is required for stabilizing the association between GluN2A and PSD95. Furthermore, p140Cap may modulate Flotillin-1 and Rac1 recruitment to the NMDAR complex and Rac1 activity (Fig. 3*B*). To assess the mechanisms through which p140Cap could regulate the composition of GluN2A-associated molecular complexes, we studied the p140Cap association with membrane LRs, which are signaling platforms enriched in cholesterol and sphingolipids, essential for the organization and compartmentalization of membrane receptor signaling components (Hering et al., 2003; Allen et al., 2007). Indeed, p140Cap has been described to be present in the fraction of membrane LR-associated proteins by two different proteomic analyses performed on rat brains (Jia et al., 2006; Suzuki et al., 2011). Moreover, the *in silico* myristoylation prediction tool for glycine myristoylation MYRbase (http://mendel.imp.ac.at/myristate/myrbase/) revealed a reliable myristylation site in p140Cap N-terminal sequence (GNAPSQDPERSSPPMLS). The myristate moiety is important for protein subcellular localization by facilitating protein–membrane as well as protein–protein interactions (Martin et al., 2011). Here, we isolated LR from mouse telencephalon, and we found that p140Cap is present in the gradient fraction enriched for LR markers Flotillin-1 and the sphingolipid GM1 (Fig. 7*A*), confirming that p140Cap is a component of the LR. However, p140Cap was also present at the high-density phases, indicating that p140Cap may localize either to raft and to non-raft compartments.

Recent studies show that the NMDAR trafficking to LR is dynamically enhanced during synaptic plasticity (Delint-Ramirez et al., 2008). Based on this evidence, we hypothesized that p140Cap could influence the recruitment or stabilization of the NMDAR subunits to synaptic LR. Since there was no difference in protein levels in synaptosomes preparation (Fig. 7*B*), we quantified the amount of NMDAR subunits recruited to WT and *p140Cap KO* synaptic LR. Synaptic LRs were purified under a specific discontinuous sucrose gradient from WT and *p140Cap KO* P2 crude synaptosomes, confirming that the total amount of synaptic LR was similar in WT and *p140Cap KO*, as reflected by the unchanged levels of LR markers (Fig. 7*C*). Indeed, in the LR from synaptosomes, both Flotillin-1 and GM1 showed the higher enrichment in Phase 4, while transferrin receptor was only present in high-density fractions (7, 8, and 9). Then we analyzed the levels of NMDAR subunits in the synaptic LR-enriched phase. Protein levels were normalized on Flotillin-1. p140Cap was present in the WT synaptic LR phase as expected (Fig. 7*D*). A significant and selective decrease of the percentage of GluN2A and PSD95 was detected in *p140Cap KO* LRs. A slight decrease was also

←

mAb. Scale bar, 20 μm. ***E***, Representative segments of dendrites (30 μm). ***F-H***, GluN2A immunostaining in combination with PSD95 in primary WT and p140Cap KO hippocampal neurons at DIV 16. Neurons were fixed with methanol. Scale bar, 20 μm. ***G***, Representative dendritic segments (30 μm) considered for the analysis of colocalization. Scale bar, 5 μm. ***H***, Percentage of colocalization between GluN2A and PSD95 in $n = 16$ dendritic segments for each experimental group ($p < 0.0001$, paired *t* test). ***I***, Immunoblotting of 30 μg extracts from DIV 16 *p140Cap KO* and WT hippocampal neurons for protein expression. Tubulin and GAPDH were used as loading control. ***J***, ***K***, DIV 16 *p140Cap KO* hippocampal neurons transfected with p140Cap-GFP (aa 1-770) and p140Cap-GFP (aa 728-1217) were fixed with methanol. Scale bar, 20 μm. ***K***, Representative dendritic segments (30 μm) measured for the analysis of colocalization. Scale bar, 5 μm. ***L***, Quantification of the percentage of colocalization between GluN2A and PSD95 in $n = 26$ dendritic segments for each experimental group ($p < 0.0001$, paired *t* test).

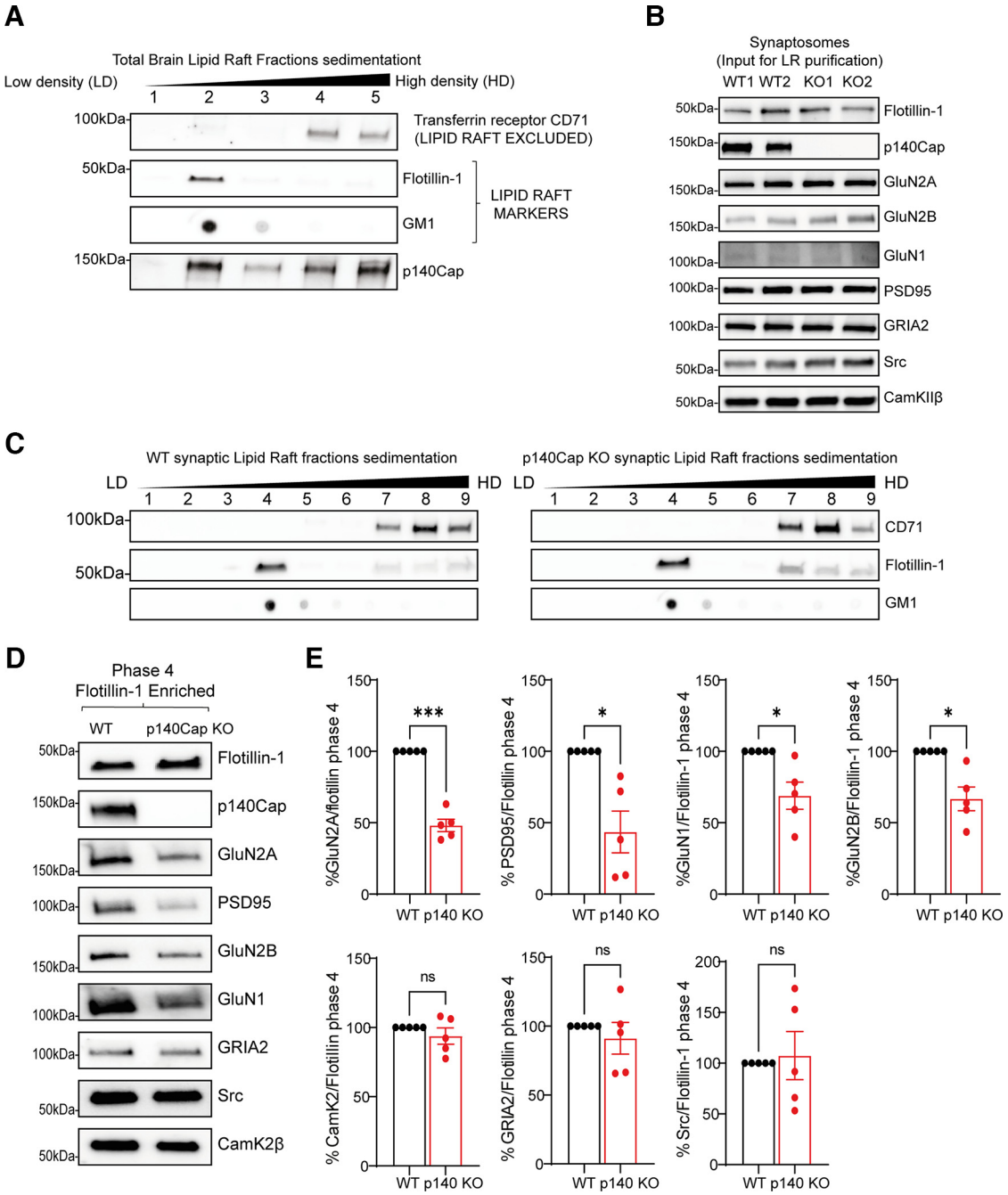

Figure 7. p140Cap affects GluN2A recruitment in synaptic LRs. ***A***, LR purification from WT telencephalon. Five fractions were obtained from the sucrose gradient, and 30 µl of each fraction was immunoblotted for the indicated proteins; 1 µl of each fraction was also assayed for the presence of the GM1 sphingolipid in a dot blot assay. ***B***, Synaptic protein expression in WT and in *p140Cap KO* P2 crude synaptosomes used to perform LR purification. Representative immunoblotting of 40 μg of WT and p140Cap KO P2 crude synaptosomes. ***C***, Synaptic LRs were isolated from WT and *p140Cap KO* P2 crude synaptosome fractions. Nine fractions were obtained, and 30 µl of each fraction was run and immunoblotted for the indicated proteins; 1 µl of each fraction was also assayed for the presence of the GM1 sphingolipid in a dot blot assay. ***D***, 30 μl of the synaptic LR-enriched phase (Phase 4) of WT and *p140Cap KO* were immunoblotted with the indicated antibodies. ***E***, Protein quantification normalized on Flotillin-1. Values are presented as a percentage of protein level with respect to the WT, paired *t* test for GluN2A $p = 0.0003$, for PSD95 $p = 0.0181$, for GluN2B $p = 0.0158$, for GluN1 $p = 0.0309$, GRIA2, Src, and Camk2β not significant; $n = 5$ mice for each experimental group.

observed for GluN2B and GluN1 subunits of NMDAR (Fig. 7*D*). Interestingly, the level of other molecules, such as the AMPAR subunit 2 (GRIA2) and the kinases Src and CamK2β, was not affected in *KO* synaptic LR (Fig. 7*E*, paired *t* test for GluN2A $p = 0.0003$, for PSD95 $p = 0.0181$, for GluN2B $p = 0.0158$, for GluN1 $p = 0.0309$, GRIA2, Src and Camk2β not significant). Therefore, the absence of p140Cap specifically alters the recruitment of specific components as NMDAR subunits, such as GluN2b and GluN1, even if these components are not directly associated to p140Cap, and of PSD95 in synaptic LR. Therefore, p140Cap can control the localization of NMDAR subunits and PSD95 into the LRs, thus resulting in improved efficiency of signal transduction given the enriched presence of signaling molecules in LR. Indeed, the localization of NMDAR into LRs could "reinforce" downstream signal transduction, facilitating the assembly of molecular complexes required for the activation of a specific signaling pathway.

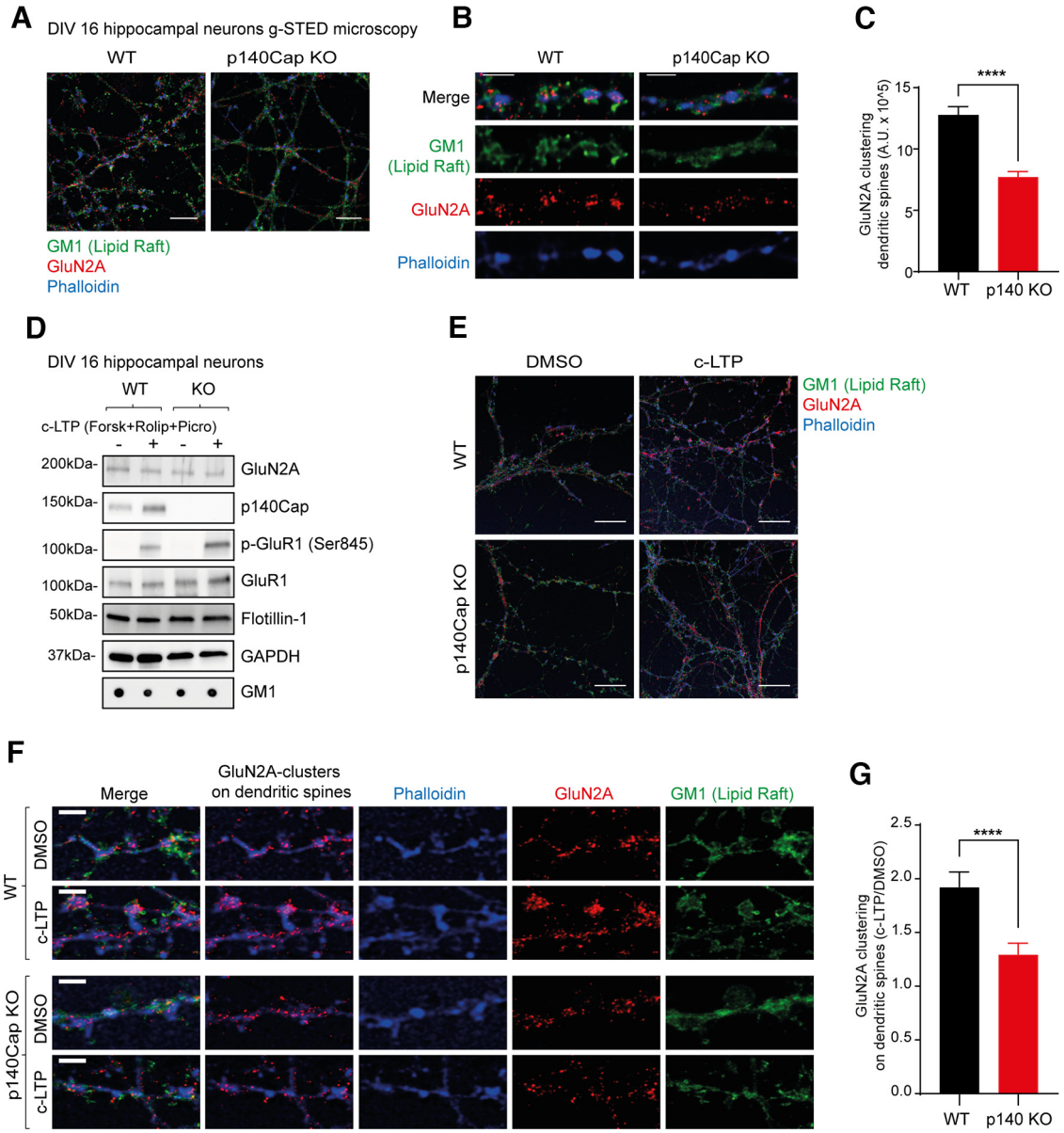

Figure 8. g-STED microscopy of GluN2A synaptic clusters in WT and *p140Cap KO* hippocampal neurons. ***A***, ***B***, g-STED microscopy of WT and *p140Cap KO* DIV 16 hippocampal neurons immunolabeled with anti-GluN2A in combination with phalloidin to visualize DS heads and Alexa-488-CTX-β for GM1 sphingolipid (LR marker). Scale bar, 10 μm. ***B***, Representative segments of dendrites (10 μm). Scale bar, 2 μm. ***C***, Quantification of GluN2A clustering on DSs (phalloidin) expressed as the ratio between the integrated density of GluN2A and the phalloidin area which corresponds to GluN2A mean of fluorescence on DSs. $n = 225$ DSs were analyzed for each genotype. $p < 0.0001$ (paired *t* test). ***D***, Immunoblotting of 30 μg WT and *p140Cap KO* hippocampal neuronal extracts on DMSO or c-LTP treatment. GAPDH was used as loading control. ***E***, ***F***, g-STED microscopy of WT and *p140Cap KO* DIV 16 hippocampal neurons on DMSO or c-LTP treatment immunolabeled as in ***A***. Scale bar, 10 μm. ***F***, Representative segments of dendrites (10 μm). ***G***, Quantification of GluN2A clustering on DSs (phalloidin) on DMSO or c-LTP, expressed as the ratio between c-LTP/DMSO for WT and *KO*; $n = 252$ DSs were analyzed for each genotype. $p < 0.0001$ (paired *t* test).

p140Cap promotes GluN2A clustering in basal condition and on c-LTP stimulation

In addition to the LR biochemical data shown above, we also investigated by g-STED microscopy whether p140Cap can control the spatial organization of GluN2A-containing NMDAR clusters in LR microdomains focusing on hippocampal neurons DS. LRs were identified with GM1 staining performed with cholera toxin subunit β, together with anti-GluN2A antibody and phalloidin-647 to visualize DS heads (Fig. 8*A*,*B*). The analysis of GluN2A clusters measured as the ratio between GluN2A signal integrated density on the DS head area showed a significantly less organization in clusters of *KO* DS compared with WT (Fig. 8*C*, $p < 0.0001$ paired *t* test). Indeed, in WT DS GluN2A clusters were completely surrounded by GM1 sphingolipids indicating that GluN2A is embedded into the LRs. Interestingly, in *KO* DS, GluN2A clusters appear smaller and more diffused to the dendritic shaft. These data confirmed a different organization of GluN2A subunit clusters and LRs in DSs in the absence of p140Cap. Moreover, differential GM1 staining in *KO* DS could suggest that p140Cap may impact also on LRs organization.

Finally, to investigate whether p140Cap can regulate NMDAR recruitment during synaptic plasticity events, we stimulated hippocampal neurons with c-LTP and performed g-STED analysis as described above. WT and *p140Cap KO* neuron stimulation was confirmed by proper p-GluR1 phosphorylation in total extracts (Fig. 8*D*, $p < 0.0001$ paired *t* test). The GluN2A or LRs markers' protein levels were similar between WT and *KO* both in basal state and on c-LTP (Fig. 8*D*). The

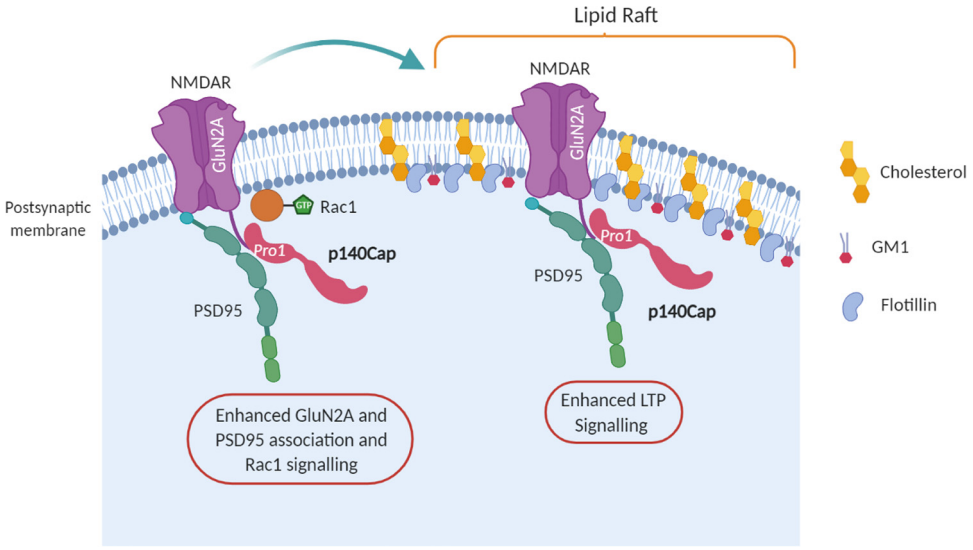

Figure 9. Model for p140Cap and GluN2A functional association in the synapse. p140Cap binds the NMDAR subunit GluN2A, thus affecting the composition of GluN2A-associated complexes, and controlling NMDAR recruitment within synaptic LRs. Left, p140Cap directly associates with the distal part of the intracellular tail of the GluN2A subunit. Moreover, p140Cap stabilizes PSD95 and GluN2A association and increases Rac1 recruitment into the GluN2A associated complex and its activation. Right, p140Cap can control the localization of GluN2A-containing NMDAR into the synaptic LRs, thus resulting in improved efficiency of LTP signal transduction. Overall, p140Cap appears as a new key adaptor protein in the PSD. However, we yet should investigate whether the favored recruitment of the pre-assembled complex of PSD95-GluN2A-p140Cap into synaptic LRs, might depend on its increased stability, on facilitation of the myristoylation process of each components, or on decreased turn-overr from the LRs. Created with www.BioRender.com.

g-STED microscopy analysis revealed that, in DS from WT primary neurons, the LR organization was unchanged after c-LTP, but the GluN2A-positive clusters were enriched compared with basal condition, confirming that c-LTP affects the GluN2A enrichment in DS (Fig. 8*E*,*F*). These data are consistent with the accumulation of GluN2A-containing NMDARs at the excitatory PSDs on c-LTP (Barria and Malinow, 2002; Grosshans et al., 2002; Bellone and Nicoll, 2007). In contrast, in DS from *p140Cap KO*, LR organization remained diffused on c-LTP, and GluN2A clusters were only slightly increased compared with the basal *KO* condition, without reaching the same density observed in the WT (Fig. 8*G*). Overall, these data confirmed that p140Cap can influence GluN2A recruitment to LR in an activity-dependent fashion during synaptic plasticity induction.

Discussion

Our previous characterization of *p140Cap KO* mice pointed out that p140Cap plays a critical role in the consolidation of new declarative memories and in the establishment of both LTP and LTD. These behavioral and electrophysiological phenotypes could depend on altered activity and turnover of ionotropic glutamate receptors (Warburton et al., 2013; Volianskis et al., 2015). Here, we demonstrate that p140Cap binds the NMDAR subunit GluN2A, thus affecting the composition of GluN2A-associated complexes, and controlling NMDAR recruitment within synaptic LRs (Fig. 9). Pull-down assay showed that the p140Cap aa 261-730, which includes the proline-rich region 1, can bind to the GluN2A C-terminal tail (aa 1349-1464), which comprises an SH3-like domain (aa 1382-1420) that is a putative binding domain for the PSD-95 family proteins (Ladépêche et al., 2014). Therefore, p140Cap could associate with GluN2A through a classical proline-rich/SH3-domain association.

The formation of chemical synapses begins during the first postnatal week, peaks at P14, and stabilizes at P21-P28, concurrent with synapse elimination and circuit refinement (Farhy-Tselnicker and Allen, 2018). Assembled GluN1/GluN2A-B receptors leave the endoplasmic reticulum and reach the synaptic membrane as part of a vesicle-associated, macromolecular complex which requires interaction with PDZ proteins (Lau and Zukin, 2007). We found that p140Cap associates with GluN2A as early as P14, when other members of the NMDAR-complex, such as PSD95 and Flotillin-1, are also recruited in the complex. Therefore, the GluN2A/p140Cap interaction appears to accompany the critical period of synaptogenesis. Furthermore, at the cellular level, p140Cap and GluN2A colocalized in mature hippocampal neurons only from DIV14 to DIV17, reinforcing the concept that the two proteins can associate during DS maturation. Interestingly, the p140Cap/GluN2A association is enhanced on synaptic activity stimulation, as is shown by c-LTP experiments. These data, together with the higher colocalization of p140Cap with the presynaptic marker Bassoon, are consistent with the observation that p140Cap is recruited into the DS, together with Endophilin 1A, in cultured hippocampal neurons during the acute phase of NMDAR-mediated cLTP (Yang et al., 2021). Indeed, the physiological NMDAR-dependent LTP induced by treating synaptosomes with glycine and KCl revealed that p140Cap is necessary to increase AMPAR insertion in the TIF, which is known to be required to sustain LTP (Corera et al., 2009). These results indicate that p140Cap is necessary for optimal chemical transmission and NMDAR-dependent LTP. The fact that p140Cap and GluN2A associate during synaptogenesis and their association is relevant for synaptic activity suggesting a possible explanation of the defective LTP observed in *p140Cap KO* mice (Repetto et al., 2014)

Scaffold proteins of the PSD bridge surface receptors with their intracellular effectors and regulate the receptors' distribution and localization both at the surface and within the PSD (Iasevoli et al., 2013). Here we demonstrate that p140Cap regulates the composition of GluN2A-associated molecular complexes. Indeed, in *p140Cap KO* synaptosomes, GluN2A was significantly less associated with the scaffold protein PSD95, the Rho-GTPase Rac1, and the LR-associated protein Flotillin-1.

This defective association could result in dysfunctional downstream signaling pathways, potentially altering the threshold for induction of NMDAR-dependent LTP, the same phenotype that was recently observed in *p140Cap KO* mice (Repetto et al., 2014). Similar changes in the composition of the NMDAR-associated molecular complex and in downstream signaling have been reported in some pathologic conditions, underlining the physiological relevance of a tight balance in the molecular effectors associated with membrane receptors (Kristiansen et al., 2006; Funk et al., 2009; Swartzwelder et al., 2016). The key role of p140Cap in NMDAR molecular complexes is also indicated by the observation that hypoxia-ischemia modifies postsynaptic GluN2B-containing NMDAR complexes in neonatal mouse brain, which is accompanied by a higher association with p140Cap (also known as SNIP) (Lu et al., 2018).

In the *p140Cap KO* synaptosomes, PSD95, the most abundant scaffold protein of the PSD, is less associated with GluN2A, suggesting that p140Cap stabilizes the association between GluN2A and PSD95. PSD95 binds to the last four amino acids (ESDV) of GluN2 subunits (Gold, 2012) and is essential to inhibit GluN2-mediated internalization (Lavezzari et al., 2004), to enhance NMDAR clustering (Kim et al., 1996) and function (Lin et al., 2004). Moreover, p140Cap associates with PSD95 in HEK293 cells independently from GluN2A, in line with our observations showing that PSD95 and p140Cap coimmunoprecipitate in mouse brain (Fossati et al., 2015) and that PSD95 takes part in the p140Cap synaptosome interactome (Alfieri et al., 2017). These data are consistent with the reduced PSD95 and GluN2A colocalization observed in *p140Cap KO* neurons. Since PSD95 and GluN2A expression levels do not change between WT and *KO* neurons, we suggest a receptor misallocation in absence of p140Cap. Overall, our data depict a scenario in which p140Cap may promote and/or stabilize GluN2A and PSD95 binding. Indeed, in the COS7 heterologous system, p140Cap expression results in increased colocalization between PSD95 and GluN2A. Moreover, the defect in GluN2A/PSD95 colocalization observed in *KO* hippocampal neurons is rescued by expressing the p140Cap domain involved in the association with GluN2A (p140Cap aa 1-770), indicating that p140Cap is required for the physiological stability of the NMDAR complexes through its interaction with GluN2A.

In *p140Cap KO* synaptosomes, Rac1 also was significantly less associated to GluN2A receptor complex, which is consistent with its reduced activation in synaptosomes. Rac1 is an important mediator of actin-remodeling of the "spinoskeleton," downstream to NMDAR activation. Moreover, Rac1 is necessary for LTP (Simons and Sampaio, 2011). Our results suggest that expression of p140Cap is necessary for localization of Rac1 in the NMDAR complex, allowing proper activation, even if we cannot exclude that p140Cap can impact on specific Rac1-GEF, such as Tiam1.

As to the functional effect of p140Cap on NMDARs, noise analysis of the NMDA currents in hippocampal neurons reveals that deleting p140Cap leads to a reduction of the unitary NMDAR current, in good agreement with the decreased I_{NMDA} amplitude measured in NMDARs expressing GluN2B rather than GluN2A subunits (Monyer et al., 1992). This effect is, however, accompanied by an increased number of NMDARs, leaving the total current unchanged. Our electrophysiological results reinforce the hypothesis that p140Cap is crucial in the recruitment of GluN2A-containing NMDARs and, consequently, in regulating NMDARs intrinsic properties.

NMDARs are distributed between the postsynaptic membrane and the LR (Hering et al., 2003), and their association with LR is developmentally regulated (Besshoh et al., 2007). LRs are nanoscopic lipid and protein microdomains enriched in cholesterol and sphingolipids, involved in protein trafficking and in cell signaling complexes (Brown and London, 1998; Simons and Toomre, 2000; Ikonen, 2001; Lingwood and Simons, 2010), critical for the maintenance and function of synapses (Sebastiao et al., 2013; Tulodziecka et al., 2016). Receptor activation and downstream signaling occurring in LRs are protected from non-raft enzymes, such as membrane phosphatases that otherwise could affect the signaling process (Simons and Toomre, 2000). Here we show that p140Cap modulates the recruitment of GluN2A-containing NMDAR in the synaptic LR. Since the putative myristoylation site in p140Cap N-terminal sequence could facilitate its recruitment to LR, we detected p140Cap in the low-density phases corresponding to the LR, as previously shown in proteomic analyses from rat brains (Jia et al., 2006; Suzuki et al., 2011). However, p140Cap is also present in the high-density phases of the gradient, with a bimodal distribution, likely playing different roles either in raft or in non-raft regions, as already described for PSD95 (Delint-Ramirez et al., 2010).

Interestingly, the synaptic LRs of *p140Cap KO* mice have a reduced level of GluN2A and PSD95, implying that p140Cap may mediate the selective enrichment of GluN2A/PSD95 in synaptic LRs, improving the efficiency of signal transduction. g-STED confocal analysis confirms the key role of p140Cap in organizing GluN2A clusters into LR of DS in hippocampal neurons. While in WT DS, GluN2A is organized in clusters embedded into the LR; in the *KO*, GluN2A clustering was significantly reduced, and the association with LR appears organized in a weaker network. The defective GluN2A clustering in LR in *p140Cap KO* was confirmed by c-LTP induction. Thus, the impaired LTP and LTD and the defects in memory and learning observed in *p140Cap KO* mice could be explained by the reduced localization of NMDARs in the synaptic LRs. Hence, p140Cap could modulate NMDAR recruitment into LR in the hippocampus during spatial learning and memory formation (Delint-Ramirez et al., 2008).

The role of p140Cap in pathologic processes or pharmacological treatments needs further investigation. Nonetheless, we notice that decreased levels of NMDAR in LRs were found in the hippocampus of a mouse model of Alzheimer's disease (Morin et al., 2016), following ischemia (Besshoh et al., 2005), or on treatment with anesthetic agents (Sierra-Valdez et al., 2016), suggesting that NMDAR reduction from LRs correlates with decreased functions.

In conclusion, we demonstrated the synaptic relevance of p140Cap as a partner of GluN2A and PSD95 proteins, which coordinate NMDAR dynamics in membrane LRs. Since NMDAR-associated proteins are implicated in synaptic dysfunction in several brain disorders, our findings point to p140Cap as a new active member of the highly dynamic synaptic network, paving the way to future studies on its involvement in neurologic and psychiatric disorders.

References

Alfieri A, Sorokina O, Adrait A, Angelini C, Russo I, Morellato A, Matteoli M, Menna E, Boeri Erba E, McLean C, Armstrong JD, Ala U, Buxbaum JD, Brusco A, Coute Y, De Rubeis S, Turco E, Defilippi P (2017) Synaptic interactome mining reveals p140Cap as a new hub for PSD proteins involved in psychiatric and neurological disorders. Front Mol Neurosci 10:212.

Allen JA, Halverson-Tamboli RA, Rasenick MM (2007) Lipid raft microdomains and neurotransmitter signalling. Nat Rev Neurosci 8:128–140.
Barria A, Malinow R (2002) Subunit-specific NMDA receptor trafficking to synapses. Neuron 35:345–353.
Bellone C, Nicoll RA (2007) Rapid bidirectional switching of synaptic NMDA receptors. Neuron 55:779–785.
Besshoh S, Bawa D, Teves L, Wallace MC, Gurd JW (2005) Increased phosphorylation and redistribution of NMDA receptors between synaptic lipid rafts and post-synaptic densities following transient global ischemia in the rat brain. J Neurochem 93:186–194.
Besshoh S, Chen S, Brown IR, Gurd JW (2007) Developmental changes in the association of NMDA receptors with lipid rafts. J Neurosci Res 85:1876–1883.
Bredt DS, Nicoll RA (2003) AMPA receptor trafficking at excitatory synapses. Neuron 40:361–379.
Brown DA, London E (1998) Functions of lipid rafts in biological membranes. Annu Rev Cell Dev Biol 14:111–136.
Caroni P, Donato F, Muller D (2012) Structural plasticity upon learning: regulation and functions. Nat Rev Neurosci 13:478–490.
Chapelle J, Baudino A, Torelli F, Savino A, Morellato A, Angelini C, Salemme V, Centonze G, Natalini D, Gai M, Poli V, Kahne T, Turco E, Defilippi P (2020) The N-terminal domain of the adaptor protein p140Cap interacts with Tiam1 and controls Tiam1/Rac1 axis. Am J Cancer Res 10:4308–4324.
Corera AT, Doucet G, Fon EA (2009) Long-term potentiation in isolated dendritic spines. PLoS One 4:e6021.
Cull-Candy S, Brickley S, Farrant M (2001) NMDA receptor subunits: diversity, development and disease. Curr Opin Neurobiol 11:327–335.
Delint-Ramirez I, Salcedo-Tello P, Bermudez-Rattoni F (2008) Spatial memory formation induces recruitment of NMDA receptor and PSD-95 to synaptic lipid rafts. J Neurochem 106:1658–1668.
Delint-Ramirez I, Fernandez E, Bayes A, Kicsi E, Komiyama NH, Grant SG (2010) In vivo composition of NMDA receptor signaling complexes differs between membrane subdomains and is modulated by PSD-95 and PSD-93. J Neurosci 30:8162–8170.
Dosemeci A, Weinberg RJ, Reese TS, Tao-Cheng JH (2016) The postsynaptic density: there is more than meets the eye. Front Synaptic Neurosci 8:23.
Esteban JA (2003) AMPA receptor trafficking: a road map for synaptic plasticity. Mol Interv 3:375–385.
Fan X, Jin WY, Wang YT (2014) The NMDA receptor complex: a multifunctional machine at the glutamatergic synapse. Front Cell Neurosci 8:160.
Farhy-Tselnicker I, Allen NJ (2018) Astrocytes, neurons, synapses: a tripartite view on cortical circuit development. Neural Dev 13:7.
Fossati G, Morini R, Corradini I, Antonucci F, Trepte P, Edry E, Sharma V, Papale A, Pozzi D, Defilippi P, Meier JC, Brambilla R, Turco E, Rosenblum K, Wanker EE, Ziv NE, Menna E, Matteoli M (2015) Reduced SNAP-25 increases PSD-95 mobility and impairs spine morphogenesis. Cell Death Differ 22:1425–1436.
Franchini L, Stanic J, Ponzoni L, Mellone M, Carrano N, Musardo S, Zianni E, Olivero G, Marcello E, Pittaluga A, Sala M, Bellone C, Racca C, Luca MD, Gardoni F (2019) Linking NMDA receptor synaptic retention to synaptic plasticity and cognition. iScience 19:927–939.
Funk AJ, Rumbaugh G, Harotunian V, McCullumsmith RE, Meador-Woodruff JH (2009) Decreased expression of NMDA receptor-associated proteins in frontal cortex of elderly patients with schizophrenia. Neuroreport 20:1019–1022.
Gardoni F, Mauceri D, Fiorentini C, Bellone C, Missale C, Cattabeni F, Luca MD (2003) CaMKII-dependent phosphorylation regulates SAP97/NR2A interaction. J Biol Chem 278:44745–44752.
Gold MG (2012) A frontier in the understanding of synaptic plasticity: solving the structure of the postsynaptic density. Bioessays 34:599–608.
Gonzalez-Lozano MA, Klemmer P, Gebuis T, Hassan C, van Nierop P, van Kesteren RE, Smit AB, Li KW (2016) Dynamics of the mouse brain cortical synaptic proteome during postnatal brain development. Sci Rep 6:35456.
Grosshans DR, Clayton DA, Coultrap SJ, Browning MD (2002) LTP leads to rapid surface expression of NMDA but not AMPA receptors in adult rat CA1. Nat Neurosci 5:27–33.
Groveman BR, Feng S, Fang XQ, Pflueger M, Lin SX, Bienkiewicz EA, Yu X (2012) The regulation of N-methyl-D-aspartate receptors by Src kinase. FEBS J 279:20–28.
Harris AZ, Pettit DL (2007) Extrasynaptic and synaptic NMDA receptors form stable and uniform pools in rat hippocampal slices. J Physiol 584:509–519.
Hayashi K, Suzuki A, Hirai S, Kurihara Y, Hoogenraad CC, Ohno S (2011) Maintenance of dendritic spine morphology by partitioning-defective 1b through regulation of microtubule growth. J Neurosci 31:12094–12103.
Hering H, Lin CC, Sheng M (2003) Lipid rafts in the maintenance of synapses, dendritic spines, and surface AMPA receptor stability. J Neurosci 23:3262–3271.
Holtmaat A, Caroni P (2016) Functional and structural underpinnings of neuronal assembly formation in learning. Nat Neurosci 19:1553–1562.
Hu XD, Huang Q, Yang X, Xia H (2007) Differential regulation of AMPA receptor trafficking by neurabin-targeted synaptic protein phosphatase-1 in synaptic transmission and long-term depression in hippocampus. J Neurosci 27:4674–4686.
Husi H, Ward MA, Choudhary JS, Blackstock WP, Grant SG (2000) Proteomic analysis of NMDA receptor-adhesion protein signaling complexes. Nat Neurosci 3:661–669.
Iasevoli F, Tomasetti C, de Bartolomeis A (2013) Scaffolding proteins of the post-synaptic density contribute to synaptic plasticity by regulating receptor localization and distribution: relevance for neuropsychiatric diseases. Neurochem Res 38:1–22.
Ikonen E (2001) Roles of lipid rafts in membrane transport. Curr Opin Cell Biol 13:470–477.
Ito H, Atsuzawa K, Sudo K, Stefano PD, Iwamoto I, Morishita R, Takei S, Semba R, Defilippi P, Asano T, Usuda N, Nagata K (2008) Characterization of a multidomain adaptor protein, p140Cap, as part of a pre-synaptic complex. J Neurochem 107:61–72.
Jaworski J, Kapitein LC, Gouveia SM, Dortland BR, Wulf PS, Grigoriev I, Camera P, Spangler SA, Stefano PD, Demmers J, Krugers H, Defilippi P, Akhmanova A, Hoogenraad CC (2009) Dynamic microtubules regulate dendritic spine morphology and synaptic plasticity. Neuron 61:85–100.
Jia JY, Lamer S, Schumann M, Schmidt MR, Krause E, Haucke V (2006) Quantitative proteomics analysis of detergent-resistant membranes from chemical synapses: evidence for cholesterol as spatial organizer of synaptic vesicle cycling. Mol Cell Proteomics 5:2060–2071.
Kim E, Cho KO, Rothschild A, Sheng M (1996) Heteromultimerization and NMDA receptor-clustering activity of Chapsyn-110, a member of the PSD-95 family of proteins. Neuron 17:103–113.
Kristiansen LV, Beneyto M, Haroutunian V, Meador-Woodruff JH (2006) Changes in NMDA receptor subunits and interacting PSD proteins in dorsolateral prefrontal and anterior cingulate cortex indicate abnormal regional expression in schizophrenia. Mol Psychiatry 11:737–747.705.
Ladépêche L, Dupuis JP, Groc L (2014) Surface trafficking of NMDA receptors: gathering from a partner to another. Seminars in cell & developmental biology 27:3–13.
Lau CG, Zukin RS (2007) NMDA receptor trafficking in synaptic plasticity and neuropsychiatric disorders. Nat Rev Neurosci 8:413–426.
Lavezzari G, McCallum J, Dewey CM, Roche KW (2004) Subunit-specific regulation of NMDA receptor endocytosis. J Neurosci 24:6383–6391.
Lin Y, Skeberdis VA, Francesconi A, Bennett MV, Zukin RS (2004) Postsynaptic density protein-95 regulates NMDA channel gating and surface expression. J Neurosci 24:10138–10148.
Lingwood D, Simons K (2010) Lipid rafts as a membrane-organizing principle. Science 327:46–50.
Lu F, Shao G, Wang Y, Guan S, Burlingame AL, Liu X, Liang X, Knox R, Ferriero DM, Jiang X (2018) Hypoxia-ischemia modifies postsynaptic GluN2B-containing NMDA receptor complexes in the neonatal mouse brain. Exp Neurol 299:65–74.
Makino Y, Johnson RC, Yu Y, Takamiya K, Huganir RL (2011) Enhanced synaptic plasticity in mice with phosphomimetic mutation of the GluA1 AMPA receptor. Proc Natl Acad Sci USA 108:8450–8455.
Monyer H, Sprengel R, Schoepfer R, Herb A, Higuchi M, Lomeli H, Burnashev N, Sakmann B, Seeburg PH (1992) Heteromeric NMDA receptors: molecular and functional distinction of subtypes. Science 256:1217–1221.
Martin DD, Beauchamp E, Berthiaume LG (2011) Post-translational myristoylation: fat matters in cellular life and death. Biochimie 93:18–31.
Moretto E, Murru L, Martano G, Sassone J, Passafaro M (2018) Glutamatergic synapses in neurodevelopmental disorders. Prog Neuropsychopharmacol Biol Psychiatry 84:328–342.

Morin JP, Diaz-Cintra S, Bermudez-Rattoni F, Delint-Ramirez I (2016) Decreased levels of NMDA but not AMPA receptors in the lipid-raft fraction of 3xTg-AD model of Alzheimer's disease: relation to Arc/Arg3.1 protein expression. Neurochem Int 100:159–163.

Niethammer M, Kim E, Sheng M (1996) Interaction between the C terminus of NMDA receptor subunits and multiple members of the PSD-95 family of membrane-associated guanylate kinases. J Neurosci 16:2157–2163.

Oh MC, Derkach VA, Guire ES, Soderling TR (2006) Extrasynaptic membrane trafficking regulated by GluR1 serine 845 phosphorylation primes AMPA receptors for long-term potentiation. J Biol Chem 281:752–758.

Otmakhov N, Khibnik L, Otmakhova N, Carpenter S, Riahi S, Asrican B, Lisman J (2004) Forskolin-induced LTP in the CA1 hippocampal region is NMDA receptor dependent. J Neurophysiol 91:1955–1962.

Paoletti P, Bellone C, Zhou Q (2013) NMDA receptor subunit diversity: impact on receptor properties, synaptic plasticity and disease. Nat Rev Neurosci 14:383–400.

Repetto D, Camera P, Melani R, Morello N, Russo I, Calcagno E, Tomasoni R, Bianchi F, Berto G, Giustetto M, Berardi N, Pizzorusso T, Matteoli M, Stefano PD, Missler M, Turco E, Cunto FD, Defilippi P (2014) p140Cap regulates memory and synaptic plasticity through Src-mediated and citron-N-mediated actin reorganization. J Neurosci 34:1542–1553.

Sala C, Segal M (2014) Dendritic spines: the locus of structural and functional plasticity. Physiol Rev 94:141–188.

Sebastiao AM, Colino-Oliveira M, Assaife-Lopes N, Dias RB, Ribeiro JA (2013) Lipid rafts, synaptic transmission and plasticity: impact in age-related neurodegenerative diseases. Neuropharmacology 64:97–107.

Sheng M, Kim E (2011) The postsynaptic organization of synapses. Cold Spring Harb Perspect Biol 3:a005678.

Shiraishi Y, Mizutani A, Mikoshiba K, Furuichi T (2003) Coincidence in dendritic clustering and synaptic targeting of homer proteins and NMDA receptor complex proteins NR2B and PSD95 during development of cultured hippocampal neurons. Mol Cell Neurosci 22:188–201.

Sierra-Valdez FJ, Ruiz-Suarez JC, Delint-Ramirez I (2016) Pentobarbital modifies the lipid raft-protein interaction: a first clue about the anesthesia mechanism on NMDA and GABAA receptors. Biochim Biophys Acta 1858:2603–2610.

Sigworth FJ (1980) The conductance of sodium channels under conditions of reduced current at the node of Ranvier. J Physiol 307:131–142.

Simons K, Sampaio JL (2011) Membrane organization and lipid rafts. Cold Spring Harb Perspect Biol 3:a004697.

Simons K, Toomre D (2000) Lipid rafts and signal transduction. Nat Rev Mol Cell Biol 1:31–39.

Siow NL, Choi RC, Xie HQ, Kong LW, Chu GK, Chan GK, Simon J, Barnard EA, Tsim KW (2010) ATP induces synaptic gene expressions in cortical neurons: transduction and transcription control via P2Y1 receptors. Mol Pharmacol 78:1059–1071.

Stanic J, Carta M, Eberini I, Pelucchi S, Marcello E, Genazzani AA, Racca C, Mulle C, Luca MD, Gardoni F (2015) Rabphilin 3A retains NMDA receptors at synaptic sites through interaction with GluN2A/PSD-95 complex. Nat Commun 6:10181.

Suzuki T, Zhang J, Miyazawa S, Liu Q, Farzan MR, Yao WD (2011) Association of membrane rafts and postsynaptic density: proteomics, biochemical, and ultrastructural analyses. J Neurochem 119:64–77.

Swanwick CC, Shapiro ME, Yi Z, Chang K, Wenthold RJ (2009) NMDA receptors interact with flotillin-1 and -2, lipid raft-associated proteins. FEBS Lett 583:1226–1230.

Swartzwelder HS, Risher ML, Miller KM, Colbran RJ, Winder DG, Wills TA (2016) Changes in the adult GluN2B associated proteome following adolescent intermittent ethanol exposure. PLoS One 11:e0155951.

Russo I, et al. (2019) p140Cap regulates GABAergic synaptogenesis and development of hippocampal inhibitory circuits. Cereb Cortex 29:91–105.

Tomasetti C, Iasevoli F, Buonaguro EF, De Berardis D, Fornaro M, Fiengo AL, Martinotti G, Orsolini L, Valchera A, Giannantonio MD, de Bartolomeis A (2017) Treating the synapse in major psychiatric disorders: the role of postsynaptic density network in dopamine-glutamate interplay and psychopharmacologic drugs molecular actions. Int J Mol Sci 18:135.

Tomasoni R, Repetto D, Morini R, Elia C, Gardoni F, Luca MD, Turco E, Defilippi P, Matteoli M (2013) SNAP-25 regulates spine formation through postsynaptic binding to p140Cap. Nat Commun 4:2136.

Traynelis SF, Jaramillo F (1998) Getting the most out of noise in the central nervous system. Trends Neurosci 21:137–145.

Tulodziecka K, Diaz-Rohrer BB, Farley MM, Chan RB, Di Paolo G, Levental KR, Waxham MN, Levental I (2016) Remodeling of the postsynaptic plasma membrane during neural development. Mol Biol Cell 27:3480–3489.

Volianskis A, France G, Jensen MS, Bortolotto ZA, Jane DE, Collingridge GL (2015) Long-term potentiation and the role of N-methyl-D-aspartate receptors. Brain Res 1621:5–16.

Warburton EC, Barker GR, Brown MW (2013) Investigations into the involvement of NMDA mechanisms in recognition memory. Neuropharmacology 74:41–47.

Yang Y, Chen J, Chen X, Li D, He J, Wang S, Zhao S, Yang X, Deng S, Tong C, Wang D, Guo Z, Li D, Ma C, Liang X, Shi YS, Liu JJ (2021) Endophilin A1 drives acute structural plasticity of dendritic spines in response to Ca^{2+}/calmodulin. J Cell Biol 220:e202007172.

Zhu J, Shang Y, Zhang M (2016) Mechanistic basis of MAGUK-organized complexes in synaptic development and signalling. Nat Rev Neurosci 17:209–223.